

STRUCTURAL CONTROLS ON KIZILDERE GEOTHERMAL FIELD,  
DENİZLİ-TURKEY

A THESIS SUBMITTED TO  
THE GRADUATE SCHOOL OF NATURAL AND APPLIED SCIENCES  
OF  
MIDDLE EAST TECHNICAL UNIVERSITY

BY

BAYKAN AKSU

IN PARTIAL FULFILLMENT OF THE REQUIREMENTS  
FOR  
THE DEGREE OF MASTER OF SCIENCE  
IN  
GEOLOGICAL ENGINEERING

AUGUST 2019



Approval of the thesis:

**STRUCTURAL CONTROLS ON KIZILDERE GEOTHERMAL FIELD,  
DENİZLİ-TURKEY**

submitted by **BAYKAN AKSU** in partial fulfillment of the requirements for the degree of **Master of Science in Geological Engineering Department, Middle East Technical University** by,

Prof. Dr. Halil Kalıpçılar  
Dean, Graduate School of **Natural and Applied Sciences**

\_\_\_\_\_

Prof. Dr. Erdin Bozkurt  
Head of Department, **Geological Engineering**

\_\_\_\_\_

Prof. Dr. Nuretdin Kaymakçı  
Supervisor, **Geological Engineering, METU**

\_\_\_\_\_

Assoc. Prof. Dr. Bora Uzel  
Co-Supervisor, **Geological Engineering, Dokuz Eylül Uni.**

\_\_\_\_\_

**Examining Committee Members:**

Prof. Dr. Erdin Bozkurt  
Geological Engineering, METU

\_\_\_\_\_

Prof. Dr. Nuretdin Kaymakçı  
Geological Engineering, METU

\_\_\_\_\_

Assoc. Prof. Dr. Bora Uzel  
Geological Engineering, Dokuz Eylül Uni.

\_\_\_\_\_

Assist. Prof. Dr. Atilla Arda Özacar  
Geological Engineering, METU

\_\_\_\_\_

Assoc. Prof. Dr. Özgür Avşar  
Geological Engineering, Muğla Sıtkı Koçman University

\_\_\_\_\_

Date: 16.08.2019

**I hereby declare that all information in this document has been obtained and presented in accordance with academic rules and ethical conduct. I also declare that, as required by these rules and conduct, I have fully cited and referenced all material and results that are not original to this work.**

Name, Surname: Baykan Aksu

Signature:

## **ABSTRACT**

### **STRUCTURAL CONTROLS ON KIZILDERE GEOTHERMAL FIELD, DENİZLİ-TURKEY**

Aksu, Baykan  
Master of Science, Geological Engineering  
Supervisor: Prof. Dr. Nuretdin Kaymakçı  
Co-Supervisor: Assoc. Prof. Dr. Bora Uzel

August 2019, 87 pages

Kızıldere geothermal field is one of the hottest fields located in south-western Anatolia and electricity has been produced from geothermal source since 1984. This high enthalpy geothermal field is located at the eastern edge of Büyük Menderes graben, which is one of the most active extensional structure belonging to the western Anatolian graben-horst system. Büyük Menderes graben, which hosts numerous geothermal fields, is a 3 - 30 km wide, 170 km long, nearly E-W trending depression developed under the N-S directed crustal strain. The study area includes four different continental sedimentary packages separated by regional unconformities.

Play type of Kızıldere geothermal field is developed within an extensional domain where heat is supplied by the percolation of cold meteoric water that heated up at depth and recharges the system. In order to identify structural control of this field, geological mapping and characterization of the faults were performed. Three types of faults, which played a role on the geothermal system were identified. These are approximately E-W striking high angle normal faults, N-S striking subvertical faults and a low angle old detachment fault developed possibly prior to the development of preceding faults. In order to understand the geology and geometry of the system, in addition to field data, 76 well-data were used to develop the 3D solid model of the

Kızıldere geothermal field. Interpretations of these data showed that the intersections of N-S trending subvertical transfer faults with the E-W striking normal faults played an important role in the development of the geothermal system present in the Kızıldere geothermal field.

Keywords: South-western Anatolia, Geothermal systems, Extensional domains, Büyük Menderes graben, 3D modeling

## ÖZ

### KIZILDERE JEOTERMAL SAHASININ YAPISAL KONTROLÜ, DENİZLİ-TÜRKİYE

Aksu, Baykan  
Yüksek Lisans, Jeoloji Mühendisliği  
Tez Danışmanı: Prof. Dr. Nuretdin Kaymakçı  
Ortak Tez Danışmanı: Doç. Dr. Bora Uzel

Ağustos 2019, 87 sayfa

Kızıldere jeotermal sahası güneybatı Anadolu'nun en sıcak sahalarından biri olup 1984'den beri jeotermal kaynaktan elektrik üretimi yapılmaktadır. Bu yüksek entalpili jeotermal saha Batı Anadolu graben-horst sistemini oluşturan en aktif genişleme yapılarından biri olan Büyük Menderes grabeninin doğu ucunda bulunmaktadır. Üzerinde bir çok jeotermal saha barındıran Büyük Menderes grabeni 3 - 30 km genişliğinde, 170 km uzunluğunda, yaklaşık D-B yönlü neotektonik K-G yönlü açılma sonucu oluşmuş bir çöküntü alanıdır. Çalışma alanında bölgesel uyumsuzluklarla ayrılmış dört farklı karasal sedimentler istif bulunmaktadır.

Kızıldere jeotermal sahası, ısının yükselen ısı akısından sağlandığı fay kontrollü bir genişleme alanı olarak sınıflandırılabilir. Bu sistemlerde faylar, sistemi besleyen soğuk meteorik suların yeraltında dolanımı ve sıcak jeotermal akışkanın hareketini kontrol eder. Bu çalışma kapsamında, sahanın yapısal kontrolünü ortaya koymak için sahanın jeolojik haritalaması ve fayların nitelendirilmesi yapılmıştır. Jeotermal sistem için önemi olan üç tip fay tanımlanmıştır. Bunlar yaklaşık olarak D-B yönelimli yüksek açılı normal faylar, K-G yönelimli dikeye yakın faylar ve düşük açılı yaşlı sıyrılmaya fayıdır. Sistemin jeoloji ve geometrisini anlayabilmek için saha verilerine ek olarak 76 adet kuyu verisi Kızıldere jeotermal sahasının 3B katı modelinin

oluřturulmasında kullanılmıřtır. Toplanan tm veriler K-G ynl dikeye yakın transfer faylarla D-B ynl normal fayların keřiřiminin Kızıldere jeotermal sisteminin oluřmasında nemli rol oynadıđını gstermektedir.

Anahtar Kelimeler: Gnaybatı Anadolu, Jeotermal sistemler, Geniřleme alanı, Byk Menderes grabeni, 3B modelleme

To my parents.

## ACKNOWLEDGEMENTS

Completion and success of this thesis belong to many people whose contributions are invaluable. First and foremost, I am indebted to my supervisor Prof. Dr. Nuretdin Kaymakçı for his support, understanding and guidance through the study. I also would like to express my gratitude to my co-supervisor Assoc. Dr. Bora Uzel for his valuable contributions and his support during field studies.

I would like to thank my manager Abdülkadir Yılmaz in Zorlu Enerji Company for his trust and support, to Metin Yazman and Erinç Tonguç for being a mentor in geology. Additionally, I have great pleasure in acknowledging my gratitude to my colleagues at Zorlu Enerji, Emre Cem Emirođlu, Uđur Kaygısız, Mehmet Nazmi Kaya, Gűrhan Osmanođlu and Koray Őztűrk for being more than workmates. My very special thanks go to Muzaffer Sađanak Cavunt for being a big brother that guide me through my life and to ađdađ Yalın for his excellent computer skills.

I dedicate this work to my family and all of my friends for their unconditional support. Especially, I thank my mother with all my heart, whose dream for me was to earn this achievement. Without her endless support, patience, and love this work would not be possible.

## TABLE OF CONTENTS

ABSTRACT .....	v
ÖZ .....	vii
ACKNOWLEDGEMENTS .....	x
TABLE OF CONTENTS .....	xi
LIST OF FIGURES .....	xiv
CHAPTERS	
1. INTRODUCTION .....	1
1.1. Purpose and Scope.....	1
1.2. Method of Study .....	3
1.3. Location of the Study Area.....	4
1.4. Previous Works .....	6
1.5. Regional Tectonic Setting .....	9
2. STRATIGRAPHY .....	13
2.1. Menderes Massif .....	17
2.1.1. Core Rocks.....	18
2.1.2. Cover Rocks.....	19
2.2. Neogene Basin In-Fill .....	20
2.2.1. Kızılburun Formation .....	20
2.2.2. Sazak Formation .....	23
2.2.3. Kolankaya Formation .....	26
2.2.4. Tosunlar Formation.....	28
2.2.5. Quaternary Deposits .....	29

3. STRUCTURAL GEOLOGY .....	31
3.1. N-S Trending Faults.....	33
3.1.1. Gebeler Fault .....	33
3.1.2. Karataş Fault.....	35
3.1.3. Demirtaş Fault .....	37
3.1.4. Pelitliada Fault.....	38
3.1.5. Payamlık Fault.....	39
3.1.6. Minor Faults .....	40
3.2. E-W Trending Faults.....	42
3.2.1. Gökdere Fault .....	43
3.2.2. Fault 1 .....	44
3.2.3. Fault 2.....	45
3.2.4. Fault 3.....	47
3.2.5. Fault 4.....	47
3.2.6. South Margin Faults .....	49
4. 3D STRUCTURAL-GEOLOGICAL MODELING .....	51
4.1. 3D Lithological Model.....	52
4.1.1. Modeling Metamorphic Rocks .....	52
4.1.2. Modeling Kızılburun and Sazak Formations.....	53
4.1.3. Modeling Kolankaya Formation .....	56
4.1.4. Modeling Tosunlar Formation and Recent Deposits.....	57
4.2. 3D Structural Model.....	59
4.2.1. E-W Trending Faults .....	59
4.2.2. N-S Trending Faults .....	62

4.3. 3D Thermal Model .....	65
5. DISCUSSIONS.....	69
6. CONCLUSION.....	73
REFERENCES.....	75

## LIST OF FIGURES

Figure 1-1. a) Simplified tectonic map of Turkey (Barka, 1992). NAFS: North Anatolian Fault System, EAFS: East Anatolian Fault System, DSFS: Dead Sea Fault System. b) Geological map of western Turkey (Bozkurt, 2000). CMM: Central Menderes Massif, SMM: Southern Menderes Massif, NMM: Northern Menderes Massif. ....	5
Figure 1-2. Schematic cross-sections illustrating consecutive stages of the tectonic evolution of western Anatolia (Yılmaz, 2017). ....	11
Figure 2-1. Stratigraphic comparison of the present study and previous studies compiled near Kızıldere geothermal field. ....	13
Figure 2-2. Geological map of the study area.....	15
Figure 2-3. The generalized tectono-stratigraphic column of the study area. ....	16
Figure 2-4. Geology map of western Anatolia showing its main tectonic components (Yılmaz, 2017). DG = Demirci graben; GG = Gördes graben; SG = Selendi graben; UG = Uşak-Ulubey graben; BEG = Bergama graben; GDG = Gediz graben; BMG = Büyük Menderes graben SOG = Soma graben; DP = Dilek Peninsula; Sö G = Söke graben; BH = Bozdağ horst; ÖG; Ören Graben, YG; Yatağan Graben, KT; The Kale-Tavas basin, LN; Lycian Nappes, LNF; Lycian nappe front , A, C, D, Iz and M; cities of Aydın, Çanakkale, Denizli, İzmir, Manisa and Muğla.....	17
Figure 2-5. Close-up view of core rocks near Old Savcılı Village (see Figure 2-2. for its location). ....	18
Figure 2-6. Generalized stratigraphic section of the Menderes Massif prior to the metamorphism and deformation (Candan et al., 2011; Yılmaz, 2017). ....	19
Figure 2-7. Close-up view of boulder-block conglomerates of Kızılburun Formation northeast of Cankurtaran Hill (see Figure 2-2. for its location). ....	21
Figure 2-8. Close-up view of limestone-coal alternation of Kızılburun Formation north of the Gökdere Fault (see Figure 2-2. for its location). ....	22

Figure 2-9. Close-up view of gradual contact between the upper part mudstones of Kızılburun Formation and clayey limestones of Sazak Formation northeast of Cankurtaran Hill (see Figure 2-2. for its location). .....	23
Figure 2-10. Close-up view of yellow-white colored clayey limestone and brown-colored claystone alternation of Sazak Formation near Örenli (see Figure 2-2. for its location). .....	24
Figure 2-11. General view of massive limestones of Sazak Formation near Örenli (see Figure 2-2. for its location). .....	25
Figure 2-12. View of fumaroles on limestone units of Sazak Formation in Gebeler Valley (see Figure 2-2. for its location). .....	26
Figure 2-13. Close-up view of bioclastic limestones of Kolankaya Formation near Orta Hill (see Figure 2-2. for its location). .....	27
Figure 2-14. Close-up view of unconformity surface between Kolankaya Formation and Tosunlar Formation near Orta Hill (see Figure 2-2. for its location). .....	28
Figure 2-15. Close-up view of pebble-boulder conglomerates of Tosunlar Formation near Aşşağitekke Village (see Figure 2-2. for its location). .....	29
Figure 3-1. Structural map of the study area draped over the Digital Elevation Model (DEM). Paleostress locations and plots are also included. ....	32
Figure 3-2. A) General view of the surface of Gebeler Fault; B) Close-up view of two overprinting sets of slickenlines in Gebeler Valley (see Figure 3-1 for its location). R1: Older set showing dextral strike-slip faulting; R2: Younger set showing normal faulting. ....	34
Figure 3-3. Two sets of slickenlines measured from Gebeler Fault and paleostress reconstruction using Angelier's direct inversion method on Schmidt's lower hemisphere. (White arrow: $\sigma_3$ ; Grey arrow: $\sigma_2$ ; Black arrow: $\sigma_1$ ; Black dot: $\sigma_1$ vertical; Grey dot: $\sigma_2$ vertical) .....	35
Figure 3-4. A) General view of the surface of Karataş Fault; B) Close-up view of slickenlines on Karataş Fault on Sütleğenli Valley (see Figure 3-1 for its location). .....	36
Figure 3-5. Slickenlines measured from Karataş Fault and paleostress reconstruction using Angelier's direct inversion method on Schmidt's lower hemisphere. (White	

arrow: $\sigma_3$ ; Grey arrow: $\sigma_2$ ; Black arrow: $\sigma_1$ ; Black dot: $\sigma_1$ vertical; Grey dot: $\sigma_2$ vertical).....	36
Figure 3-6. A) General view of the surface of Demirtaş Fault; B) and C) Close-up view of slickenlines on Demirtaş Fault on Kavak Valley (see Figure 3-1 for its location).....	37
Figure 3-7. Slickenlines measured from Demirtaş Fault and paleostress reconstruction using Angelier’s direct inversion method on Schmidt’s lower hemisphere. (White arrow: $\sigma_3$ ; Grey arrow: $\sigma_2$ ; Black arrow: $\sigma_1$ ; Black dot: $\sigma_1$ vertical; Grey dot: $\sigma_2$ vertical).....	38
Figure 3-8. A) General view of the surface of Pelitliada Fault; B) Close-up view of slickenlines on Pelitliada Fault on Kavak Valley (see Figure 3-1 for its location). ..	39
Figure 3-9. General view of Payamlık Fault scarp near Payamlık Hill (see Figure 3-1 for its location).....	40
Figure 3-10. General view of Fault B surface near Cankurtaran Valley (see Figure 3-1 for its location).....	41
Figure 3-11. A) General view of the surface of Gökdere Fault; B) Close-up view of slickenlines on Gökdere Fault; C) Close-up view of brecciated surfaces on Gökdere Fault (see Figure 3-1 for its location). .....	43
Figure 3-12. Slickenlines measured from Gökdere Fault and paleostress reconstruction using Angelier’s direct inversion method on Schmidt’s lower hemisphere. (White arrow: $\sigma_3$ ; Grey arrow: $\sigma_2$ ; Black arrow: $\sigma_1$ ; Black dot: $\sigma_1$ vertical; Grey dot: $\sigma_2$ vertical).....	44
Figure 3-13. Panoramic view of the Fault 1 scarp near İmam Mountain (see Figure 3-1 for its location).....	45
Figure 3-14. A) General view of the Fault 2 scarp; B) Close-up view of slickenlines on Fault 2 along the Cankurtaran Stream (see Figure 3-1 for its location). .....	46
Figure 3-15. Slickenlines measured from Fault 2 and paleostress reconstruction using Angelier’s direct inversion method on Schmidt’s lower hemisphere. (White arrow: $\sigma_3$ ; Grey arrow: $\sigma_2$ ; Black arrow: $\sigma_1$ ; Black dot: $\sigma_1$ vertical; Grey dot: $\sigma_2$ vertical).....	46

Figure 3-16. A) General view of the surface of Fault 4; B) Close-up view of slickenlines on Fault 4 near Örenli (see Figure 3-1 for its location).....	48
Figure 3-17. Slickenlines measured from Fault 4 and paleostress reconstruction using Angelier’s direct inversion method on Schmidt’s lower hemisphere. (White arrow: $\sigma_3$ ; Grey arrow: $\sigma_2$ ; Black arrow: $\sigma_1$ ; Black dot: $\sigma_1$ vertical; Grey dot: $\sigma_2$ vertical) .....	48
Figure 3-18. Step-like morphology observed in the southern margin of the Büyük Menderes graben (see Figure 3-1 for its location.....)	49
Figure 4-1. The output volume of the metamorphic rocks. (Looking northeast, 250-meter contour spacing). The yellow-colored line is the boundary between gneiss and other metamorphic rocks.....	52
Figure 4-2. The output volumes of metamorphic rocks and gneiss. The black-colored surface represents the Pelitliada Fault. (Looking North, 250-meter contour spacing) .....	53
Figure 4-3. Well-data showing the lateral extent of Kızılburun and Sazak Formations. (Looking northeast, 250-meter contour spacing).....	54
Figure 4-4. The output volume of Kızılburun Formation. The black-colored surface represents the Pelitliada Fault. (Looking north, 250-meter counter spacing) .....	55
Figure 4-5. The output volume of Sazak Formation. The black-colored surface represents the Pelitliada Fault. (Looking north, 250-meter counter spacing) .....	55
Figure 4-6. The output volume of Kolankaya Formation. (Looking north, 250-meter counter spacing) .....	56
Figure 4-7. Cut-out section showing the onlap surface of older deposits and their stratigraphic relation with Kolankaya Formation. (Looking north-northwest).....	57
Figure 4-8. Finalized 3D lithological model of the Kızıldere geothermal field. (Looking north).....	57
Figure 4-9. Finalized 3D lithological model of the Kızıldere geothermal field. (Looking south).....	58
Figure 4-10. Finalized 3D lithological model of the Kızıldere geothermal field. (Looking east) .....	58

Figure 4-11. Finalized 3D lithological model of the Kızıldere geothermal field. (Looking west).....	59
Figure 4-12. Modeled fault planes of Fault 1 (white-colored surface) and Fault 2 (red-colored surface). Pink colored dots are mud loss intervals encountered in Fault 1 that was used to edit the surface of the fault. (Looking north).....	60
Figure 4-13. Modeled fault planes along the northern margin of the Büyük Menderes graben (White-colored surface: Fault 1; Red-colored surface: Fault 2; Green-colored surface: Fault 3; Yellow-colored surface: Fault 4; Pink-colored surface: Gökdere Fault). (Looking northwest).....	60
Figure 4-14. Modeled fault planes along the southern margin of the Büyük Menderes graben (White-colored surface: SF-1; Blue-colored surface: SF-2; Orange-colored surface: SF-3). (Looking southeast) .....	61
Figure 4-15. Structural model of E-W trending normal faults. (Looking west).....	62
Figure 4-16. Structural modeling of Gebeler Fault Zone (Red-colored surfaces: Antithetic Fault A and B; Orange-colored surfaces: Synthetic Fault C and D; White-colored surface: Main Fault-Gebeler Fault). (Looking North).....	63
Figure 4-17. Structural model of N-S trending faults. (Red-colored surfaces: Gebeler Fault Zone; Green-colored surface: Karataş Fault; Pink-colored surface: Demirtaş Fault; Yellow-colored surface: Pelitliada Fault). (Looking north).....	63
Figure 4-18. Cross-section showing major N-S trending faults. 800-meter offset was calculated along Pelitliada Fault (Black-colored line: Pelitliada Fault; Green-colored line: Demirtaş Fault; Red-colored lines: Gebeler Fault Zone; Blue-colored line: Karataş Fault). (Looking North).....	64
Figure 4-19. Final 3D structural model of the Kızıldere geothermal field (Red-colored surfaces: E-W trending normal faults along the northern margin of the Büyük Menderes graben; Grey-colored surfaces: E-W trending normal faults along the southern margin of the Büyük Menderes graben; Yellow-colored surfaces: Gebeler Fault Zone; Green-colored surfaces: Other N-S trending faults). (Looking north)...	65
Figure 4-20. Thermal distribution of the Kızıldere geothermal field. ....	66

Figure 4-21. E-W cross-section of the thermal and structural model of the Kızıldere geothermal field (Green-colored surfaces: Gebeler Fault Zone; Black-colored surfaces: From east to west Karataş, Demirtaş and Pelitliada faults; Navy blue-colored surfaces: E-W trending faults). (Looking south).....66



## CHAPTER 1

### INTRODUCTION

#### 1.1. Purpose and Scope

Turkey is located within the Alpine-Himalayan Orogenic Belt, a tectonically active belt with rich geothermal energy resources that are mainly used for electricity production, heating of greenhouses and residences, industry, thermal and health tourism. Electricity production from geothermal energy in 2018 had reached 1144 MW and 78% of the geothermal fields are centered in western Anatolia (Republic of Turkey Ministry of Energy and Natural Resources, 2018). Kızıldere geothermal field is one of the most productive fields located in western Anatolia and the first electricity production from geothermal energy in Turkey started with a 15 MW power plant by TEAŞ (the Turkish Electricity Authority) in 1984. After the privatization in 2008, this field was transferred to the Zorlu Energy and currently 3 power plants with a total capacity of 260 MW is operated in this field. In addition, 60 MW power plant project is planned to be finished by Zorlu Energy in 2021.

Development of an efficient geothermal system requires components such as a) tectonically active area; b) active structures; c) heat source; d) reservoir rock with high porosity and permeability that allows percolation of geothermal fluids; e) impermeable caprock that forms a barrier above and below the reservoir rock that confines the geothermal fluids, f) geothermal fluid that can be meteoric, hydrothermal or a mixture of both. The exact heat source of western Anatolia is a highly debated subject. Magmatism in the upper crust were proposed as the source of heat for the geothermal systems (Şimsek, 1985; Filiz et al., 2000; Karamenderesi and Helvacı, 2003; Yılmazer et al., 2010; Bülbül et al., 2011; Özen et al., 2012; Özgür and Karamenderesi, 2015; Özdemir et al., 2017; Alçiçek et al., 2018). However, recent

magmatism in the area is rare or local. Only significant volcanic activity occurred in the region during Quaternary is the Kula volcanic field. On the other hand, a deeper heat source caused by slab dynamics (asthenospheric mantle uplift due to slab rollback and back-arc spreading) were also proposed (Kaya, 2015; Koçyiğit, 2015; Roche et al., 2015, 2016, 2018; Gessner et al., 2017). Geothermal system present in the western Anatolia can be classified as an extensional domain where magmatism is absent or little in terms of heat source and heat is mainly supplied by extensional or transtensional tectonics (Moeck, 2014). Crustal thinning and upwelling asthenosphere are the main reasons for elevated heat flow values ( $\sim 100 \text{ mW m}^{-2}$ ) experienced at shallow depths throughout the Aegean domain (Erkan, 2014, 2015).

Kızıldere is one of the active, high-enthalpy, structurally controlled geothermal field located in the western part of Büyük Menderes graben. E-W trending low angle detachment fault, N-E striking subvertical, mainly strike-slip faults and E-W trending high angle normal faults are the major structures that play a key role in this geothermal field. The region has a long history of compressional and extensional deformation, which reactivated some of the older faults with new characteristics (Şengör, 1987). This resulted in a complex interaction and development history of the faults in the region which requires very meticulous analysis of the surface and subsurface data to unravel the characteristics of faults that played a role in the underground percolation of geothermal fluids.

In this study, we have followed and integrated approach that combines detailed field observations with the well-data. All of this information were used to develop 3D solid models of the study area, which helped to better understand the geometry and relationships between various lithologies and structures observed in the Kızıldere geothermal field.

## **1.2. Method of Study**

The study is carried out in four stages, namely previous works, field work, analysis of borehole data and office works. Previous works consist of reviewing available literature and initial analysis of the study area.

Field work part of the study started with the 1/25000 scale geological mapping of the study area. This part was performed to understand stratigraphic and tectonic contacts, reservoir and caprock properties. During the mapping, faults were identified and any slickenline measurements were recorded. Fault plane data, which consists of dip, strike, rake angles and sense of movement, were later analyzed with Win-Tensor software developed by Delvaux and Sperner (2003) and the paleostress configurations were reconstructed. Faults without any kinematic indicators on the fault plane were also recorded and their off-set senses were identified by using geological and geomorphological off-set features. Additionally, alteration zones, hot springs and fumaroles which could indicate geothermal activity were mapped and documented at the field.

In the third stage, data from 76 wells, ranging from 500 to 4000 m depth, were included in the study. Well-data includes lithology, drilling mud loss values and static temperature readings with respect to depth. Cuttings collected during drilling were analyzed with a stereomicroscope for lithologic determinations.

As a final stage, the fieldwork and the borehole data were integrated and analyzed together. Results of the integration were used to develop 3-D lithological (solid model), structural and thermal model of the study area by using Seequent Leapfrog Geo v.4.4.2 software. In this stage, seismic sections, which could not be presented here due to confidentiality, interpreted by Zorlu Energy Company were used to verify the 3-D structural model of the field. Finally, these models were used to interpret structural control of the geothermal field and identify favorable spots for geothermal exploration.

### **1.3. Location of the Study Area**

The study area is located in the eastern end of Büyük Menderes graben between 37.59 N - 37.54 N latitudes and 28.45 E - 28.53 E longitudes (Figure 1-1). It is placed on M21b1 and M21b2 coded 1/25000 topographical maps and covers an area around 107 km<sup>2</sup>. Study area shows typical graben-horst topography where step-like morphology can be observed along the northern and southern margin of Büyük Menderes graben.

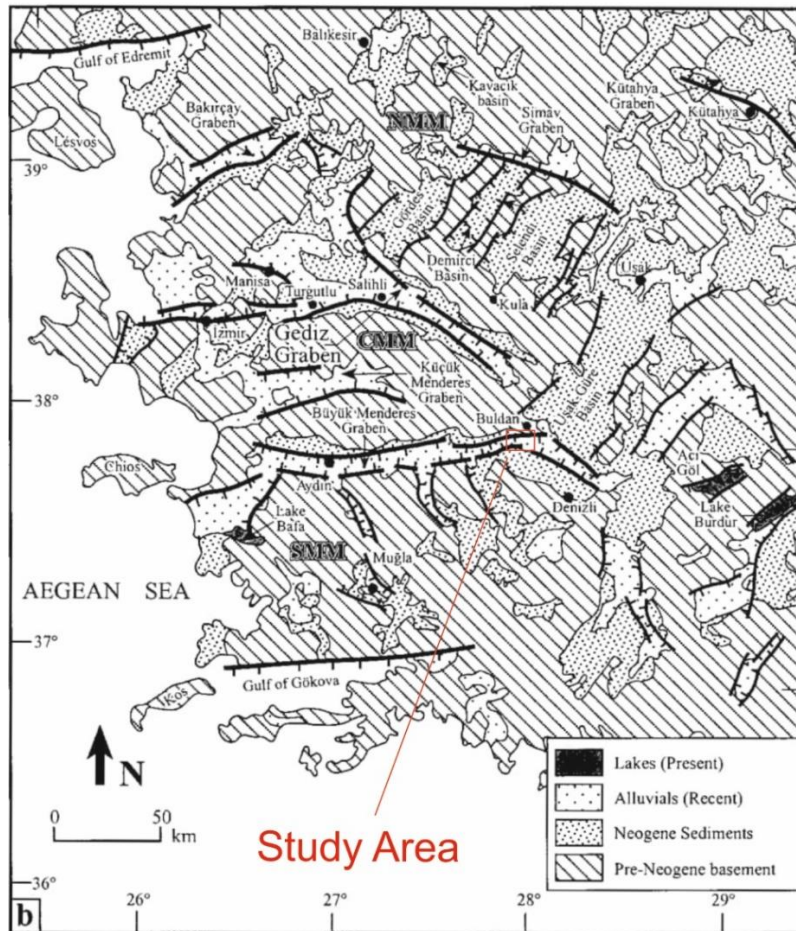
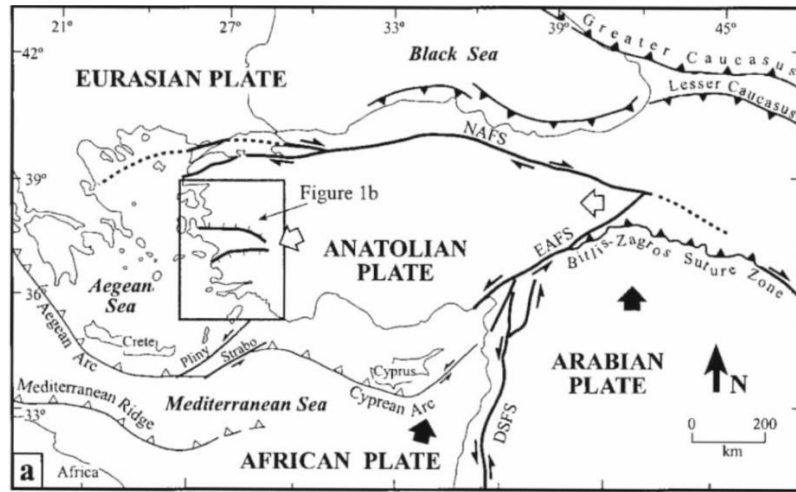


Figure 1-1. a) Simplified tectonic map of Turkey (Barka, 1992). NAFS: North Anatolian Fault System, EAFS: East Anatolian Fault System, DSFS: Dead Sea Fault System. b) Geological map of western Turkey (Bozkurt, 2000). CMM: Central Menderes Massif, SMM: Southern Menderes Massif, NMM: Northern Menderes Massif.

#### **1.4. Previous Works**

Western Anatolia has been one of the most broadly studied regions in Turkey due to its unique extensional tectonic characteristics. After the commencement of guaranteed feed-in tariff for renewable energy, geothermal studies increased dramatically in Turkey. Geothermal exploration requires multi-disciplinary knowledge which includes basin analysis, tectonics, structural geology, stratigraphy, geophysics, geochemistry, and hydrogeology. Previous works carried out in the vicinity of the Kızıldere geothermal field were summarized in this section.

Rock units exposed in the Kızıldere geothermal field were firstly studied in detail on a scale of 1/25000 by Şimşek (1984), who worked in the region covering Denizli M21-b1-b2-b4 and Uşak L21-c3, c-4 map sections. His study investigated the geothermal potential of the field and he identified Kızılburun and Kolankaya Formations as caprock, while Sazak Formation and brittle rocks of the Menderes Massif as reservoir rocks. He reported that youngest and major faults were E-W and NW-SE trending graben faults that control the geothermal system. On the other hand, N-S directional normal faults were also identified as older faults that are cut and displaced by these graben faults.

Sun (1990) updated the geological map of Şimşek (1984) while studying the lignite potential of the region between Uşak and Denizli. In his study, he aged Kızılburun and Sazak Formations as Late Miocene.

Westaway (1993) studied the Neogene evolution of the Denizli region and claimed that Miocene aged red conglomerates were deposited before the N-S extension began. He also proposed the main active faulting in Büyük Menderes graben migrated from south to north between 4-5 Ma.

Cohen et al. (1995) suggested that the Neogene sediments in the Büyük Menderes and Gediz grabens are syn-tectonic and these grabens developed as a half-graben.

Bozkurt (2000) studied the timing of extension in Büyük Menderes graben and proposed that Büyük Menderes graben exhibits two-stage extension. Age of the second N-S extension was initiated during Pliocene which also coincides with the start of the slip on the North Anatolian Fault.

Kaymakçı (2006) studied the kinematic development of Denizli Basin and proposed two extension directions; NE-SW and NW-SE. Based on paleostress data he suggested that these two extension directions are active from Late Miocene to recent and they interchange frequently through time.

Alçıçek et al. (2007) investigated the Neogene sedimentary rocks around Denizli and made detailed facies analysis. Graben fill of Denizli Basin was initiated by the Babadağ fault located at the southern part of Büyük Menderes graben. Based on isotope geochemistry of  $\delta^{18}\text{O}$  they claimed that Early - Middle Miocene aged Kızılburun Formation deposited under humid climatic conditions in an alluvial distal-mid fan environment. Depositional environment of Middle Miocene - Late Miocene aged Sazak Formation was much more arid and saline which represents a lake environment. The depositional environment changed into a deep brackish lake during the deposition of Late Miocene - Late Pliocene aged Kolankaya Formation.

Gürer et al. (2009) studied the development of Büyük Menderes graben. In this study two set of faults were measured: 1) NE and NW trending subvertical oblique faults, and 2) E-W directed normal faults. They reported that NE and NW trending faults both limit the extension of Late - Middle Miocene and control the deposition. On the other hand, E-W trending faults were found adjacent to strata deposited in current graben configuration. Upper Pliocene - Upper Pleistocene rocks both cover Miocene units and metamorphic rocks with angular unconformity suggesting that Miocene rocks were not deposited in the E-W trending graben.

Faulds et al. (2009) compared and characterized the geothermal fields in western Turkey including Kızıldere geothermal field and Great Basin in the USA. Two types of faults that control Kızıldere geothermal field were parallel E-W striking south-

dipping normal faults and NE striking subvertical transverse faults. They also reported that Kızıldere geothermal field stands on the eastern edge of Büyük Menderes graben where normal faults lose displacement and change into splays further enhancing permeability and porosity of the rocks.

Çifçi et al. (2011) worked on the seismic sections located west of the Kızıldere geothermal field near Nazilli and claimed that Büyük Menderes graben is a supradetachment basin where deposition of the Miocene units was controlled by E-W striking Büyük Menderes detachment fault. Seismic data also showed that this detachment fault has a listric geometry and turns horizontal at 10 km depth. They also recognized N-S striking strike-slip faults in the area and proposed that they evolved after the development of the Büyük Menderes graben.

Koçyiğit (2015) studied geothermal systems in the Büyük Menderes and classified them as fault-controlled non-magmatic systems. The heat source for these systems are zones of shallow curie points at depths of 8 -11.5 km where crustal extension and rise of asthenosphere occurred. Most of the hot water springs are located in the Büyük Menderes detachment zone which implies that it is still being used for these geothermal systems. Secondly, high angle normal faults that cut the detachment fault share the circulation of meteoric water and upwelling geothermal fluids. He proposed that well-aimed drilling at the intersection of high angle normal faults and the detachment fault would yield higher potential in terms of geothermal exploration.

Kaya (2015) investigated the Ortakçı and Kızıldere geothermal field in Büyük Menderes graben. He reported that main structures controlling the heat and flow transfer are: 1) Relay ramp areas of normal faults; 2) intersection of N-S trending cross faults and high angle normal faults; 3) termination of major normal faults with horsetail structure; 4) nearly parallel extensional cracks developed in front of major faults. In addition, kinematic analysis of faults showed an NNE - SSW extension direction.

Roche et al. (2018) reported that isotopic studies of hot spring waters located in Büyük Menderes detachment zone show contents of mantle volatiles. Detachment fault plays the first-order control on geothermal systems with their deep roots. Fluids migrate from the deep crust by both thermal-buoyancy mechanism and deformation mechanism, where the heat is generated by tectonic activity.

### **1.5. Regional Tectonic Setting**

Turkey is located in the Alpine-Himalayan belt, which formed during the closure of the Tethys Ocean from Mesozoic to Cenozoic, and involved the collision of African, Arabian, Anatolian and Eurasian plates (Bozkurt and Mittwede, 2001). Plate boundaries spanning Turkey are South Aegean - Cyprian subduction zone, the sinistral Dead Sea Fault, East Anatolian and North Anatolian transform fault systems. According to Eurasia-fixed Global Positioning System (GPS) velocities, the Arabian plate moves north at a rate of 8 mm/yr near South Aegean-Cyprus Arc while western Anatolia moves southwestward at a rate of 35 mm/yr (McClusky et al., 2000). The relative motion between these plates indicates the south-westward retreat of the trench which was caused by roll-back of the slab beneath Anatolia (Le Pichon and Angelier, 1979; Moores et al., 1984; Royden, 1993; Govers and Fichtner, 2016). The collision between the Arabian plate and Eurasia occurs from the 15 mm/yr northward movement of the Arabian plate relative to Eurasia (Kahle et al., 1998). Anatolian plate escapes towards southwest from this collision at a rate of 20 mm/yr through North Anatolian and East Anatolian fault systems (Şengör, 1979; Oral et al., 1992; Reilinger et al., 1997; McClusky et al., 2000).

Neotectonics of the western Anatolian extensional province is mainly characterized by the N-S extension and E-W trending graben-horst systems intervened with NE-SW grabens. Origin of the grabens and the mechanism of the extension and age of this extension in western Anatolia has long been subjected to debate. Four main models

were proposed: 1) Westward escape of the Anatolian Plate; 2) Back-arc spreading model; 3) Orogenic collapse model; 4) Episodic two-stage graben model.

Westward escape of the Anatolian plate model suggests that the northward movement of the Arabian Plate and collision along the Bitlis-Zagros suture triggered the westward movement of the Anatolian plate (Şengör, 1979; Şengör and Kidd, 1979). Oceanic lithosphere of the African plate subducts into Anatolian-Aegean plate. Initiation age of this subduction is still debated and vary from about 12 my (Dewey and Şengör, 1979; Şengör, 1979) to 7 my (Westaway, 2003, 2004), 5 my (Barka and Kandinsky-Cade, 1988; Armijo et al., 1999; Barka, 1992; Westaway, 1994a and b), and 4 my, end of Pliocene (Şaroğlu and Yılmaz, 1991).

Back-arc spreading model is based on the southward slab pull on the Anatolia Plate from the subduction of the eastern Mediterranean oceanic lithosphere under the Aegean-Anatolian plate. Southward migration of the Hellenic volcanic arc initiated and back-arc extension commenced in the overlying plate (McKenzie, 1970, 1972, 1978; Jackson and McKenzie, 1988; Le Pichon and Angelier, 1981; Meijer and Wortel, 1997; Jolivet et al., 2003, 2013; Philippon et al., 2014). Repeated rollbacks were identified along with the downgoing slab, and the rate of the rollback is estimated to be up to 3 cm/yr (Philippon et al., 2014).

Orogenic collapse model proposes that the cause of the spreading and thinning of overthickened crust is the collision and ongoing tectonic uplift (Dewey, 1988). As a consequence of this collision and N-S shortening, the crust reached to a thickness of more than 50-55 km at the end of the Eocene (Şengör et al., 1985; Rimmerle et al., 2003). This resulted in the uplift of the crust and after the convergence stopped the thick crust began to spread and thin resulting in the orogen to collapse. This was followed by a regional north-south extension and tectonic uplift (Dewey and Şengör, 1979; Şengör, 1979; Dewey, 1988; Dewey et al., 1989).

Episodic two-stage graben model suggested two different episodes of extension and a short-lived compression (Bozkurt and Park, 1994; Koçyiğit et al., 1999; Bozkurt,

2002; Yılmaz et al., 2000; Koçyiğit and Özacar, 2003; Bozkurt and Sözbilir, 2004; Purvis and Robertson, 2004, 2005; Bozkurt and Rojay, 2005; Koçyiğit, 2005; Yılmaz, 2017). The first extension in the Aegean-western Anatolia occurs after the orogenic collapse (Burchfiel et al., 2003, 2008) and this was followed by a compressional phase presumed to be initiated by a change in the kinematics of Eurasian and Arabian plates. The second N-S extensional period was started by the westward escape of the Anatolian plate due to seafloor spreading of the Red Sea (Hempton, 1987).

Evolution of the Western Anatolia and E-W trending grabens from Late Cretaceous to Quaternary can be summarized in 6 stages (Figure 1-2).

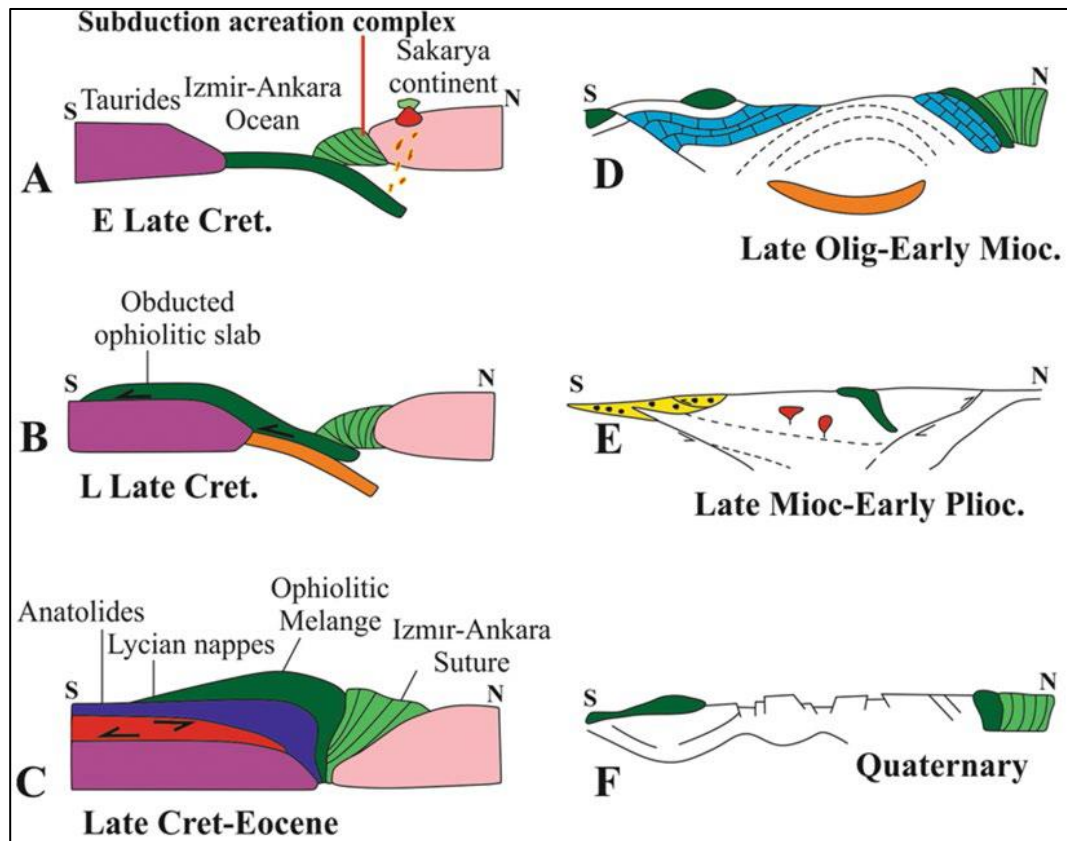


Figure 1-2. Schematic cross-sections illustrating consecutive stages of the tectonic evolution of western Anatolia (Yılmaz, 2017).

- a) The closure of the northern branch of the Tethys Ocean (İzmir-Ankara Ocean) started the convergence period between Taurides and Sakarya continents in Early Late Cretaceous (Şengör and Yılmaz, 1981; Yılmaz, 1981; Yılmaz et al., 1995; Yılmaz, 2017).
- b) Thrusting and emplacement of ophiolitic slabs metamorphosed the subducting Tauride/Anatolide plate and formed the future Menderes Massif (Yılmaz, 1981).
- c) Movement of giant nappe packages and ophiolitic slabs from north to south by thrust tectonics continued between Late Cretaceous to Eocene, forming/deforming the metamorphic rocks of Menderes Massif (Yılmaz, 2017). After that, these metamorphic rocks were started to uplift at the Late Eocene - Oligocene (Yılmaz, 1997; Burchfiel et al., 2003; Lacassin et al., 2007).
- d) Western Anatolia and Menderes Massif suffered a north-south compressional deformation between Late Oligocene - Early Miocene (Yılmaz, 2017). As a result of this high-grade metamorphic rocks were thrust and emplaced above the metamorphic cover rocks. Compression stage ended due to the collapse of the orogeny and a new extensional phase began. During this extension approximately NE-SW trending grabens formed and Lower Miocene terrestrial sediments deposited directly on metamorphic and ophiolitic rocks (Yılmaz, 2017).
- e) A regional erosion occurred during the Late Miocene - Early Pliocene period. Both metamorphic rocks and NE-SW trending graben fills were covered by interconnected lakes that act as a regional caprock. Bozdağ Dome uplifted by the development of Bozdağ detachment fault (Yılmaz, 2017).
- f) As a result of the current N-S extension in the Western Anatolia, during Pliocene - Quaternary period E-W trending grabens superimposed on the E-W and NE-SW Miocene basins resulting into the current morphology (Yazman et al., 1998; Temel et al., 2004; Uzel et al., 2012).

## CHAPTER 2

### STRATIGRAPHY

The rock units crop out near Kızıldere geothermal field were studied previously by various researchers (Şimşek, 1984; Sun, 1990; Bozkurt, 2000; Kaymakçı, 2006; Alçiçek et al., 2007; Gürer et al., 2009; Koçyiğit, 2015). However, there is no agreement on the naming and ages of the units in the region (Figure 2-1).

Age		Şimşek (1984)	Sun (1990)	Bozkurt (2000)	Kaymakçı (2006)	Alçiçek et al. (2007)	Gürer et al. (2009)	Koçyiğit (2015)	This Study		
Quaternary	Holocene	Alluvium, Travertine	Alluvium, Travertine	Unit C	Quaternary Units	Alluvium, Travertine	Unit C Subunit B2	Feslek Fm.	Alluvium, Alluvial Fan		
	Pleistocene		Asartepe Fm.			Tosunlar Fm.	Subunit B1	Tosunlar Fm.	Tosunlar Fm.		
Pliocene	Late Gelasian Piacenzian	Tosunlar Fm.	Ulubey Fm.	Unit B	Pliocene Units	Kolankaya Fm.	Stratigraphic Gap	Stratigraphic Gap	Kolankaya Fm.		
		Kolankaya Fm.	Kolankaya Fm.								
	Early Zanclean	Sazak Fm.	Kolankaya Fm.								
		Kızılburun Fm.									
Miocene	Late Messinian Tortonian	Menderes Massif	Sazak Fm.	Stratigraphic Gap	Late Miocene Units		Stratigraphic Gap	Stratigraphic Gap	Sazak Fm.		
			Kızılburun Fm.								
	Middle Serravalian Langhian		Menderes Massif	Menderes Massif	Unit A	Early -Middle Miocene Units	Kızılburun Fm.	Subunit A2	Kızılburun Group	Kızılburun Fm.	
	Early Burdigalian Aquitanian						Subunit A1	Menderes Massif	Menderes Massif		
Pre-Miocene		Menderes Massif					Menderes Massif	Menderes Massif	Menderes Massif	Menderes Massif	Menderes Massif

Figure 2-1. Stratigraphic comparison of the present study and previous studies compiled near Kızıldere geothermal field.

In this thesis, we have not conducted any detailed stratigraphical or sedimentological study in the area since they are outside the scope of this work, but in order to get a better understanding of the stratigraphic contacts, reservoir and caprock properties and petrologic description of cutting samples field geology was essential. A geological map of the study area at the 1/25000 scale was created (Figure 2-2).

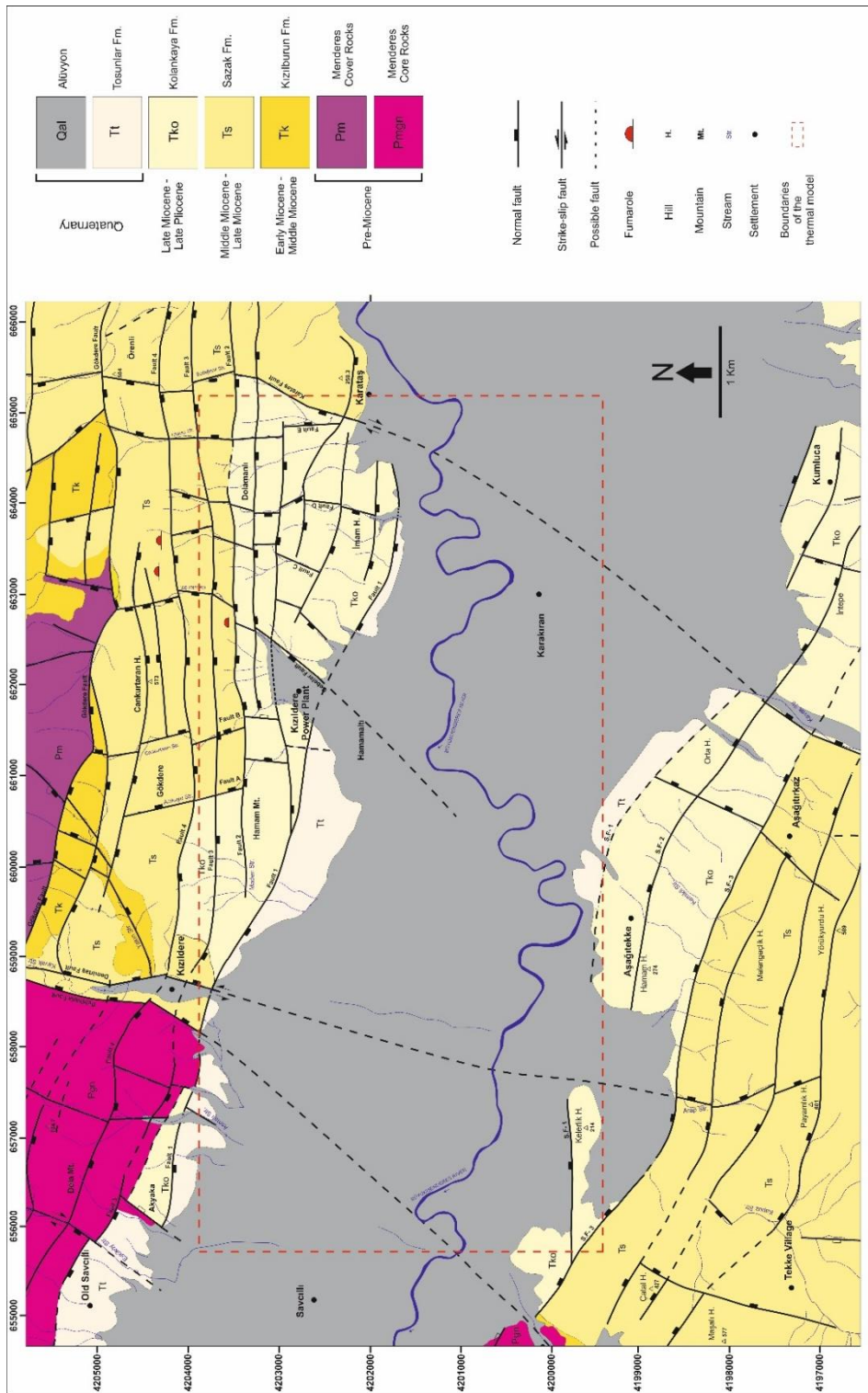


Figure 2-2. Geological map of the study area.

Stratigraphy of the study area from oldest to youngest includes the Menderes Massif, Kızılburun Formation, Sazak Formation, Kolankaya Formation, Tosunlar Formation and Quaternary aged alluvium deposits (Figure 2-3). Rocks exposed near Kızıldere geothermal field are subdivided into two basic categories: (1) Menderes Massif, (2) Neogene Basin In-Fill.

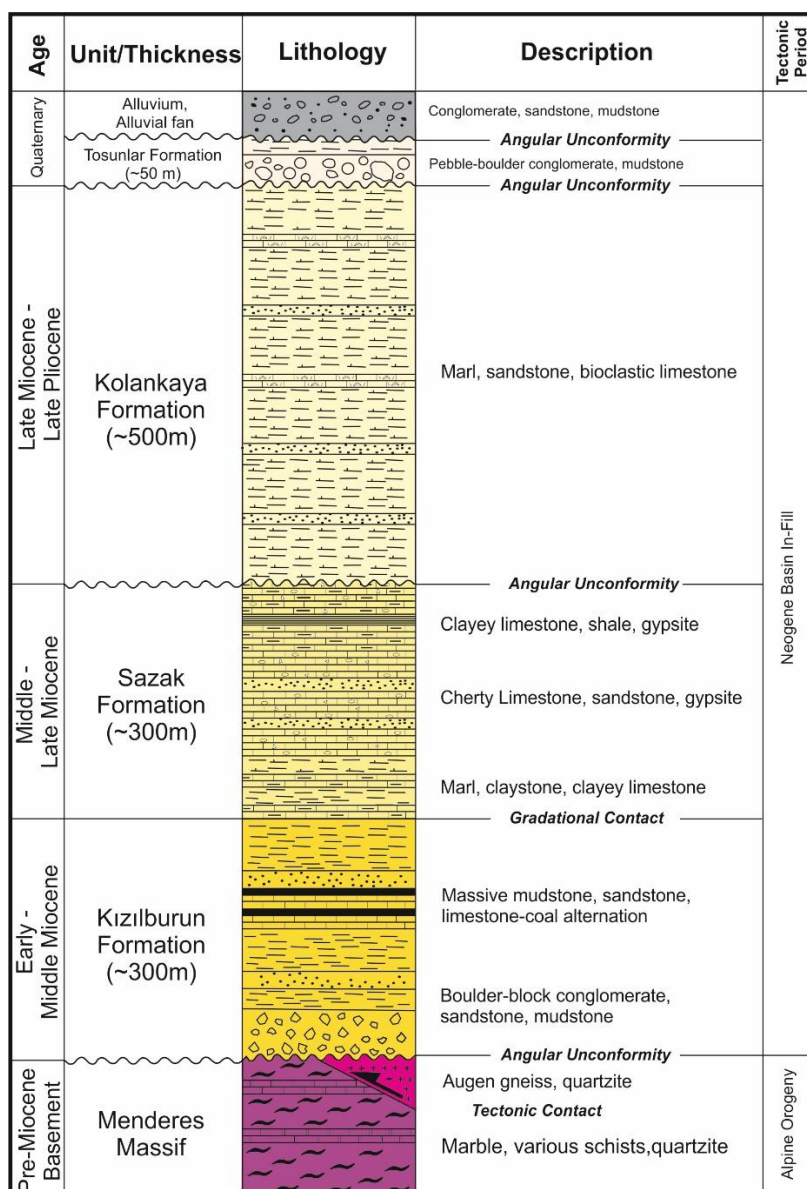


Figure 2-3. The generalized tectono-stratigraphic column of the study area.

## 2.1. Menderes Massif

The Menderes Massif, first identified and named by Philipson (1918), is the largest tectonic unit of western Anatolia. This metamorphic massif is located between the Izmir-Ankara suture in the north and the Taurides in the south (Figure 2-4). The Menderes Massif consists of two different metamorphic rock assemblages: a) core rocks; b) cover rocks (Bozkurt and Oberhansli, 2001; Candan et al., 2011).

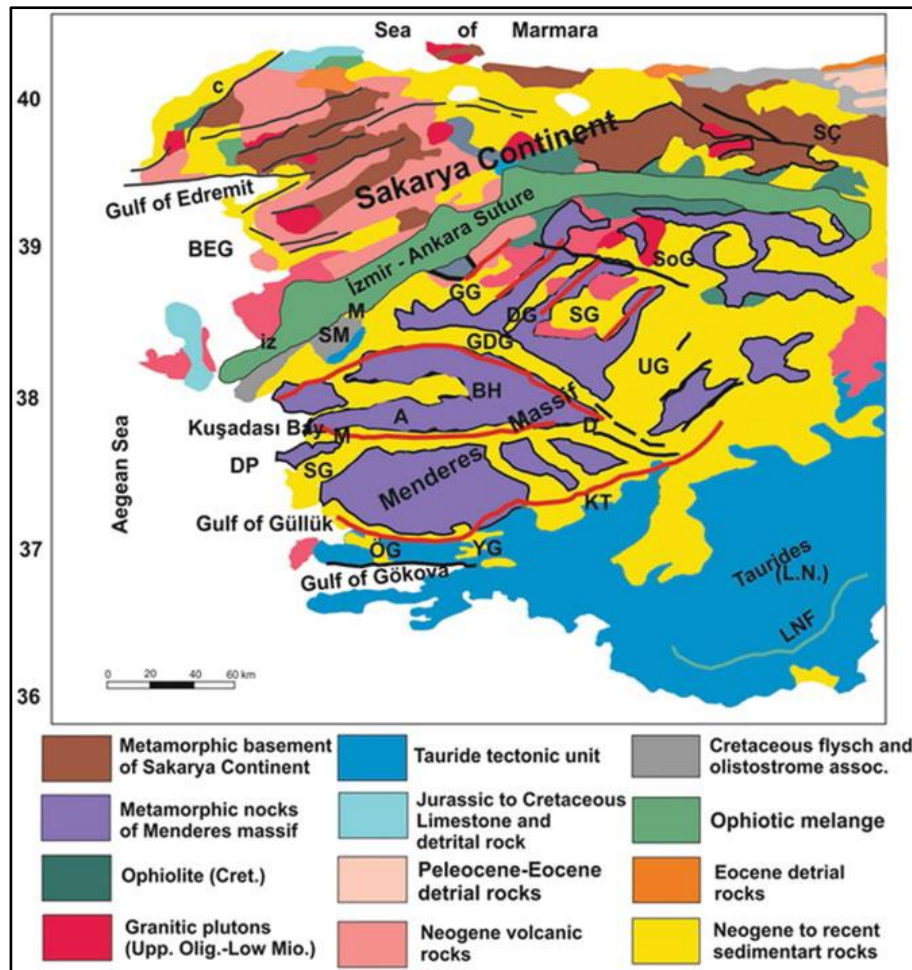


Figure 2-4. Geology map of western Anatolia showing its main tectonic components (Yılmaz, 2017). DG = Demirci graben; GG = Gördes graben; SG = Selendi graben; UG = Uşak-Ulubey graben; BEG = Bergama graben; GDG = Gediz graben; BMG = Büyük Menderes graben SOG = Soma graben; DP = Dilek Peninsula; Sö G = Söke graben; BH = Bozdağ horst; ÖG; Ören Graben, YG; Yatağan Graben, KT; The Kale-Tavas basin, LN; Lycian Nappes, LNF; Lycian nappe front, A, C, D, Iz and M; cities of Aydın, Çanakkale, Denizli, İzmir, Manisa and Muğla.

### 2.1.1. Core Rocks

Core rocks of the Menderes Massif are generally composed of augen gneiss, quartzite, metagranite and other high pressure/high temperature metamorphic rocks of Pan-African basement (550 - 520 Ma) (Şengör et al., 1984; Candan et al., 2001, 2011; Erdoğan and Güngör, 2004; Bozkurt and Oberhansli, 2001; Oberhansli et al., 2010). In the study area and throughout Büyük Menderes graben these pan-African basement rocks are observed as tectonic slices that thrust over cover rocks.

In the study area, core rocks expose towards the west of the Kızıldere Village (Figure 2-2). In addition, cutting samples and cores showed that these high P-T rocks thicken toward west and range between 300 - 1000 meters. Studied augen gneiss are generally very coarse-grained, brittle, highly fractured, extensively weathered and sheared (Figure 2-5). Porosity and permeability of these rocks are high due to multiple deformations occurred and they are one of the suitable reservoir rocks for geothermal fluid accumulation in the Kızıldere geothermal field.



Figure 2-5. Close-up view of core rocks near Old Savcılı Village (see Figure 2-2. for its location).

### 2.1.2. Cover Rocks

The second major rock assemblage of the Menderes Massif consists of low-grade various schists, phyllites, quartzite, and marble. Schists include garnet-bearing mica-schist, calc-schist, quartz-muscovite-schist, and chlorite-schist. Two marble bearing rock assemblages were identified. These are observed either as schist-marble intercalation or massive. Age of this massive marble was determined as Mesozoic while the other cover rocks were aged as mostly Paleozoic (Boray, 1982; Konak, 2002; Konak and Şenel, 2002; Şengor et al., 1984; Bozkurt and Oberhansli, 2001; Gessner et al., 2011; Candan et al., 2011). The original succession of Menderes Massif was disturbed due to multiple deformations and metamorphism but the reconstruction of Menderes Massif can be displayed in Figure 2-6.

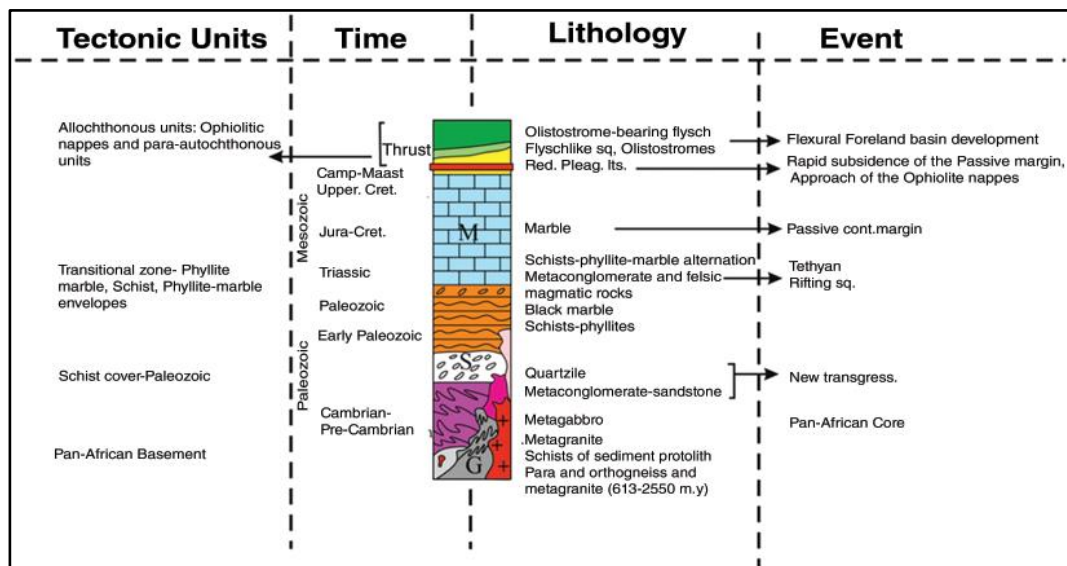


Figure 2-6. Generalized stratigraphic section of the Menderes Massif prior to the metamorphism and deformation (Candan et al., 2011; Yılmaz, 2017).

In the study area, cover rocks excluding the massive marble exposures within the footwall of Gökdere Fault (Figure 2-2). Borehole data suggested valuable information about the cover rocks. Thrusting was highly active within these rocks and it is almost

impossible to correlate cover rocks from the drilling cuttings due to this extensive thrusting. For this reason, Menderes Massif should be viewed as a combination of different tectonic slices.

## **2.2. Neogene Basin In-Fill**

In the study area, the basin-fill rocks are represented by the Kızılburun, Sazak, Kolankaya, Tosunlar formations and Quaternary alluvium deposits.

### **2.2.1. Kızılburun Formation**

Kızılburun formation was first defined and named by Şimşek (1984). Its type locality is the Kızılburun Hill located north of the study area. Early Miocene - Early Middle Miocene aged (Alçıçek et al., 2007) Kızılburun Formation rests with an angular unconformity on cover and core rocks of Menderes Massif. The lower part of Kızılburun Formation can be characterized as matrix-supported, unsorted, polygenetic, boulder-block conglomerates with red-brown colored mudstone and sandstone intercalations. The grain size of the conglomerate ranges between a few millimeters to several meters and shows a gradual decrease towards the top of the formation (Figure 2-7).



Figure 2-7. Close-up view of boulder-block conglomerates of Kızılburun Formation northeast of Cankurtaran Hill (see Figure 2-2. for its location).

Clasts are generally angular and consist of metamorphic rock pieces. Bedding planes are hardly visible and thickness ranges up to 2 meters. Conglomerates gradually pass into sandstone and mudstone alternation. Sandstones are pale yellow-red colored, medium bedded, poorly sorted, medium-coarse grained and with no visible grading. Mudstones are red-brown colored, medium bedded and with silty levels. Sedimentary deposits in the lower part of Kızılburun Formation indicate a high energy fault-controlled environment deposited as a proximal-mid alluvial fan (Alçıçek et al., 2007).

The upper part of Kızılburun Formation consists of massive red-colored mudstones, laminated siltstone-sandstone, conglomerates and thin limestones alternating with coal. Compared to the lower part, grain size is generally finer in the upper part, beddings become clearer and show a fining upward grading. Limestones are beige-brown colored, thin-thick bedded, micritic and alternate with coal (Figure 2-8). Coals are black-dark brown colored, thick-very thick-bedded (up to 3 meters) with organic

plant remains. The upper part of the Kızılburun Formation deposited as a distal fan where fluvial deposition is much more dominant (Alçıçek et al., 2007).



Figure 2-8. Close-up view of limestone-coal alternation of Kızılburun Formation north of the Gökdere Fault (see Figure 2-2. for its location).

Kızılburun Formation exposes on the northern flank of the Büyük Menderes graben towards the south of the Gökdere Fault (Figure 2-2). Borehole data show similar lithologies and most of the facies were identified. According to both field observations and borehole data, this formation was limited by the Pelitliada Fault and it is absent towards west of the Kızıldere Village. Kızılburun Formation is a good caprock for this geothermal system because of the low permeable mudstone levels.

### 2.2.2. Sazak Formation

This unit was first defined and named by Şimşek (1984). Its type locality is the Old Sazak Village located northeast of the study area. Age of this formation was determined as Middle Miocene - Early Late Miocene (Alçiçek et al., 2007) and Sazak Formation rest conformably on Kızılburun Formation (Figure 2-9).



Figure 2-9. Close-up view of gradual contact between the upper part mudstones of Kızılburun Formation and clayey limestones of Sazak Formation northeast of Cankurtaran Hill (see Figure 2-2. for its location).

The lower part of Sazak Formation can be characterized by grey-green colored marl, brown-colored claystone and clayey limestone alternations. Marls are generally thin-medium bedded and parallel laminated. Clayey limestones are yellow-white colored, medium to thick-bedded with occasional fossil content while claystones are thin-bedded, with silty and organic-rich levels (Figure 2-10).



Figure 2-10. Close-up view of yellow-white colored clayey limestone and brown-colored claystone alternation of Sazak Formation near Örenli (see Figure 2-2. for its location).

The middle part of Sazak Formation consists of massive limestones alternating with sandstones. Limestones are generally light brown-colored, very thick-bedded, massive, karstic, partially dolomitized and contain thin chert and gypsum layers (Figure 2-11). Gypsum content generally increases towards the top of this formation which indicates an increase in evaporative conditions. Sandstones are white-grey colored, medium bedded, medium to fine-grained, well-sorted and consolidated with carbonate cement.



Figure 2-11. General view of massive limestones of Sazak Formation near Örenli (see Figure 2-2. for its location).

The upper part of this formation is composed of clayey limestones and organic-rich calcareous shale facies. Carbonate shales are white-beige colored, very thin laminated and with organic-rich intervals. Rocks observed on the lower part of Sazak Formation indicate a deep lake environment while through the upper part anhydrite content and limestone advance indicate a low energy, very arid, shallower lacustrine environment.

Distribution of Sazak Formation is wide and exposes both in north and south flank of the Büyük Menderes graben (Figure 2-2). Borehole data show similar lithologies and most of the facies were identified. Similar to the Kızıldere Formation, Sazak Formation is also limited towards the west of the Kızıldere Village with the Pelitliada Fault. In terms of the geothermal system, this formation provides an excellent reservoir because of its karstic nature and brittle rheology. Hot springs and fumaroles were identified on limestone units of the Sazak Formation in the study area (Figure 2-2, 2-12).



Figure 2-12. View of fumaroles on limestone units of Sazak Formation in Gebeler Valley (see Figure 2-2. for its location).

### **2.2.3. Kolankaya Formation**

This unit was first defined and named by Şimşek (1984). Its type locality is the Kolankaya Hill located east of the study area. Age of this formation was determined as Middle Late Miocene - Late Pliocene (Alçiçek et al., 2007). Kolankaya Formation rests unconformably on both Menderes Massif and Sazak Formation. This formation can be characterized by laminated marl and rare occasions of sandstone and bioclastic limestone intercalations. Marls are generally grey-white colored, parallel laminated to thick-bedded with gypsum layers and occasional fossil content (Figure 2-13). On the other hand, bioclastic limestones are light grey-yellow colored and composed of abundant fossil fragments with carbonate cement.



Figure 2-13. Close-up view of bioclastic limestones of Kolankaya Formation near Orta Hill (see Figure 2-2. for its location).

Marl deposits indicate a much deeper, low energy lacustrine environment with brackish water conditions compared to the Sazak Formation (Alçiçek et al., 2007). Kolankaya Formation outcrops both in the northern and southern margin of the Büyük Menderes graben (Figure 2-2). Borehole data is slightly different than field observations. Generally, the thickness of this marl dominated formation is around 400 meters (up to 774 m in some wells). However, during the field study, no such thick marl outcrop was found. Probably, this formation was extensively weathered due to its high susceptibility to weathering. Unlike Kızıldere and Sazak formations, Kolankaya Formation passes through the west of the Kızıldere Village and rests with unconformity on core rocks of the Menderes Massif. In terms of the geothermal system, this formation is an excellent caprock because of its high thickness, lateral continuity and low permeability.

#### 2.2.4. Tosunlar Formation

This unit was first defined and named by Şimşek (1984). Its type locality is the Tosunlar Village located northeast of the study area. Age of this formation was defined as Early Quaternary (Sarica, 2000; Sözbilir and Emre, 1990; Kaymakçı, 2006) and Tosunlar Formation covers all of the older rocks with a regional unconformity (Figure 2-14).

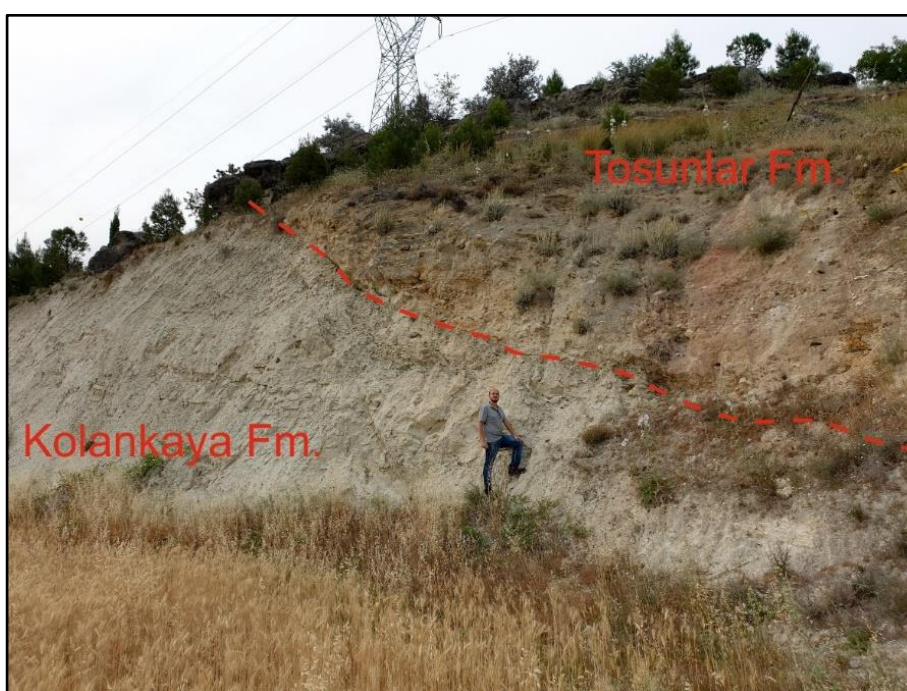


Figure 2-14. Close-up view of unconformity surface between Kolankaya Formation and Tosunlar Formation near Orta Hill (see Figure 2-2. for its location).

Tosunlar Formation consists of yellow-brown colored, polygenetic, poorly sorted, pebble-boulder conglomerate and occasional mudstone intercalations (Figure 2-15). Generally, grain size ranges from pebble to boulder while the clasts are subrounded and composed of metamorphic rocks of Menderes Massif and limestone clasts of

Neogene basin in-fill units. Beddings are weakly developed with erosional bases and rock is poorly consolidated with a sandy matrix.



Figure 2-15. Close-up view of pebble-boulder conglomerates of Tosunlar Formation near Aşşagıtekke Village (see Figure 2-2. for its location).

Tosunlar Formation deposited as a fault-controlled high energy debris flow on mountain fronts. In the study area, Tosunlar Formation exposes on both flanks of Büyük Menderes graben, in front of NE-SW and E-W trending normal faults (Figure 2-2). Borehole data show similar lithologies with field observations.

#### **2.2.5. Quaternary Deposits**

Generally, these Holocene units consist of loose, poorly sorted, pebbles, sands, muds of alluvial fan and fluvial deposits. Alluvial fan deposits are found near the margins of the basin while fluvial alluvium deposits are found at the center of the basin.



## CHAPTER 3

### STRUCTURAL GEOLOGY

Faults are one of the main components of an extensional domain type geothermal system (Moeck, 2014). They have two important tasks: 1) Faults are the pathways of hot geothermal fluids and cold meteoric water that recharges the system; 2) Faulting and brittle deformation further enhance the reservoir characteristics of rocks by creating secondary porosity and permeability.

In order to understand the structural controls of the Kızıldere geothermal field, the characteristics of faults were studied in terms of geological mapping at the 1/25000 scale in the study area (Figure 3-1). Fault plane data, which include dip, strike, rake and sense of movement, were analyzed with Win-Tensor software (Delvaux and Sperner, 2003). At least 5 different samples were measured along the same fault plane in a short distance in order to create a reliable paleostress reconstruction. In these geothermal systems, the importance of the low angle detachment fault was emphasized by many researchers (Faulds et al., 2009; Koçyiğit, 2015; Kaya, 2015; Roche et al., 2018). We recognize this fault as part of the system but further investigation of the detachment fault was out of the scope of this study.

According to field mapping and observations, faults can be divided into two categories based on their trend: 1) N-S trending subvertical faults; 2) E-W trending high angle normal faults.

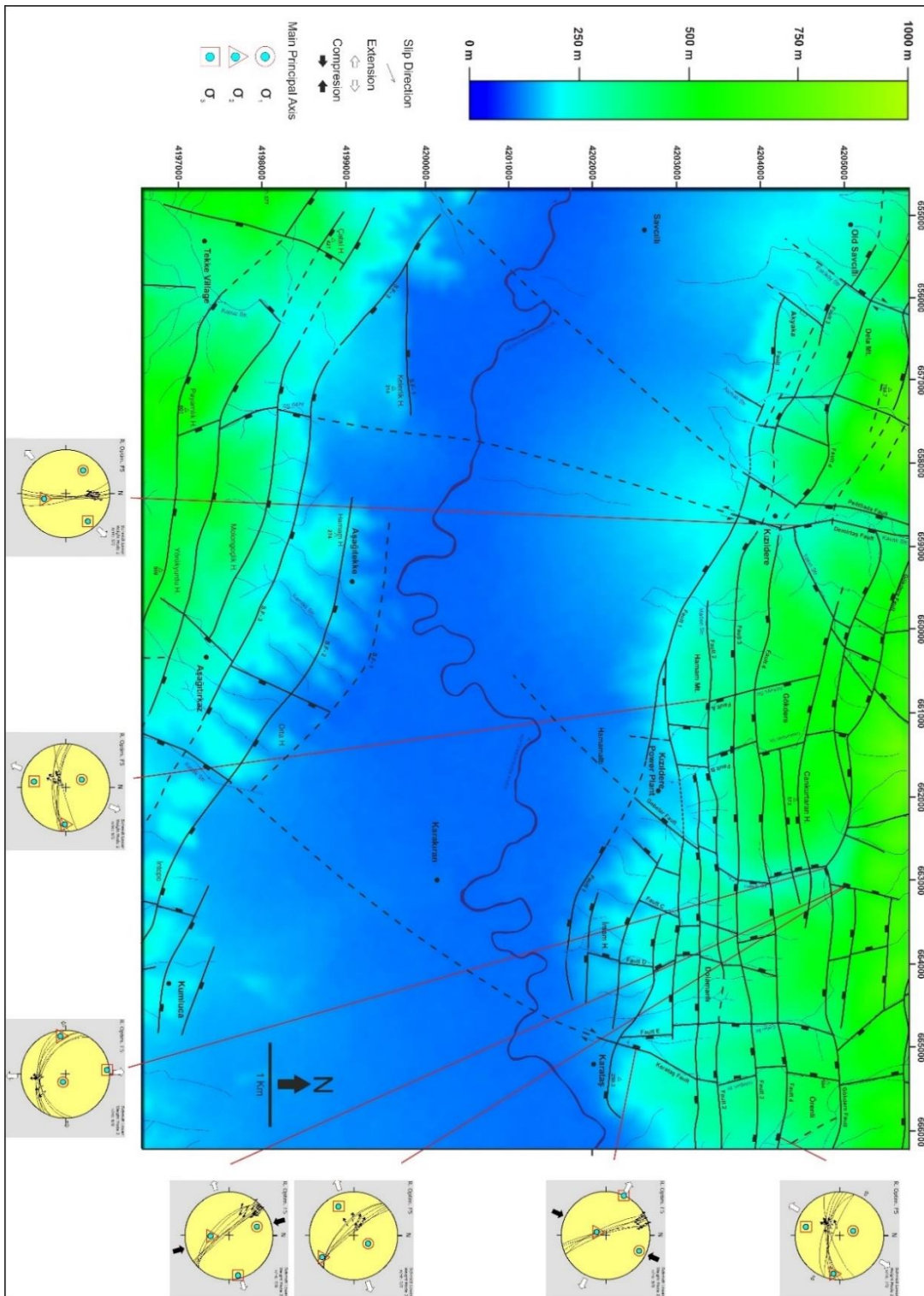


Figure 3-1. Structural map of the study area draped over the Digital Elevation Model (DEM). Paleostress locations and plots are also included.

### **3.1. N-S Trending Faults**

In the study area, these faults are NNW and NNE trending, subvertical strike-slip and oblique faults. Generally, these were cut and displaced by E-W trending faults. Best criteria to recognize these structures in the field are slickenlines, steep fault scarps, sudden changes in slope, highly deformed and brecciated rocks. These faults can be easily observed in the field by N-S directional incised valleys. Among these valleys slickenline data were obtained and photographed. In terms of geothermal activity hot springs, fumaroles, hydrothermally altered rocks were common in N-S trending faults (Figure 2-2). These incised valleys have their own drainage that supplies the system with cold meteoric water, which is transverse to the Büyük Menderes River, such as Kavak Stream, Acıkuyu Stream, Cankurtaran Stream, Gebeler Stream, Cinlisu Stream and Sütleğenli Stream (Figure 3-1). N-S trending faults are a major part of this geothermal system since they act as a conduit for both hot geothermal fluids and cold meteoric water that feeds the system. The activity of these faults is evidenced by a number of fumaroles and wells located on them, which indicate these faults are used extensively as a conduit for geothermal fluids (Figure 2-2, 2-12).

#### **3.1.1. Gebeler Fault**

Gebeler Fault is a 3.3 km long, high angle ( $60^{\circ}$ - $86^{\circ}$ ) fault that dips towards west. It starts near Kızıldere geothermal power plant with a NE trend and continues along Gebeler stream with NNW trend along the northern margin of the Büyük Menderes graben. It cuts and deforms Menderes Massif, Middle Miocene - Late Miocene Sazak Formation and Late Miocene - Late Pliocene Kolankaya Formation. On the other hand, this fault was cut and displaced by most of the E-W trending faults; resulting in a change in its trend. One of the significant displacements occurs along the intersection of Gökdere Fault, which is one of the major E-W trending faults, where the Gebeler Fault was displaced vertically and laterally (Figure 3-1). Steep fault scarps, lined hot springs and fumaroles, sudden changes in slope, deeply incised valleys and

slickenlines on fault planes were used to recognize this fault. Fault slickenlines with two overprinted sets was observed along the Gebeler Fault (Figure 3-2). Older set of slickenlines (R1), which show dextral strike-slip faulting, was crossed by normal faulting (R2).



Figure 3-2. A) General view of the surface of Gebeler Fault; B) Close-up view of two overprinting sets of slickenlines in Gebeler Valley (see Figure 3-1 for its location). R1: Older set showing dextral strike-slip faulting; R2: Younger set showing normal faulting.

Paleostress reconstruction showed that R1 set was a dextral strike-slip fault while R2 was a normal fault with NEE-NWW extension (Figure 3-3). This fault formed originally as a dextral strike-slip fault and later it reactivated to be a normal fault.

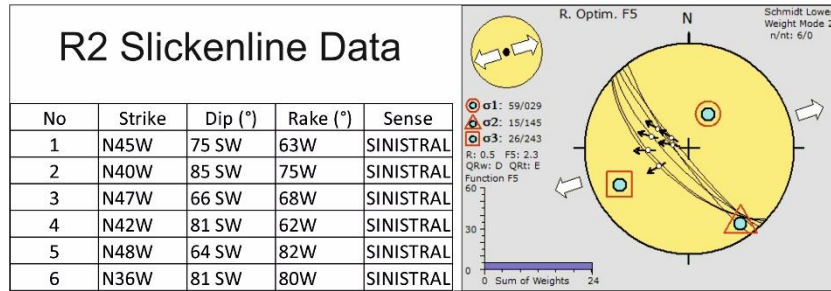
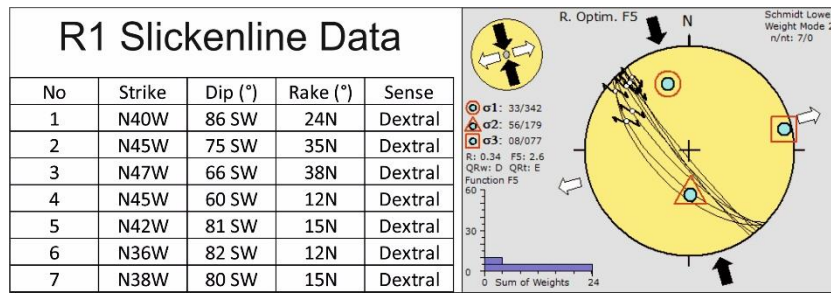


Figure 3-3. Two sets of slickenlines measured from Gebeler Fault and paleostress reconstruction using Angelier's direct inversion method on Schmidt's lower hemisphere. (White arrow:  $\sigma_3$ ; Grey arrow:  $\sigma_2$ ; Black arrow:  $\sigma_1$ ; Black dot:  $\sigma_1$  vertical; Grey dot:  $\sigma_2$  vertical)

Apart from slickenlines, 3 fumaroles were found along Gebeler Fault on limestones of Sazak Formation, which indicates this fault has a significant role on this geothermal system (Figure 2-2, 2-12).

### 3.1.2. Karataş Fault

Karataş Fault is a 4.5 km long, steep ( $76^\circ$ - $80^\circ$ ) dextral strike-slip fault that dips towards west. It starts from Karataş Village with NNE trend and continues along Sütleğenli stream with NNW to N-S trend along the northern margin of the Büyük Menderes graben. It cuts and juxtaposes Middle Miocene - Late Miocene Sazak Formation and Late Miocene - Late Pliocene Kolankaya Formation. Similar to the Gebeler Fault, this fault was also cut and displaced by most of the E-W trending faults; resulting in a change in its trend. Steep fault scarps, sudden changes in slope, deeply incised valleys and slickenlines were used to recognize this fault (Figure 3-4).



Figure 3-4. A) General view of the surface of Karataş Fault; B) Close-up view of slickenlines on Karataş Fault on Sütüğeçenli Valley (see Figure 3-1 for its location).

Paleostress reconstruction showed that Karataş Fault is a dextral strike-slip fault with high  $\sigma_2$  values (Figure 3-5).

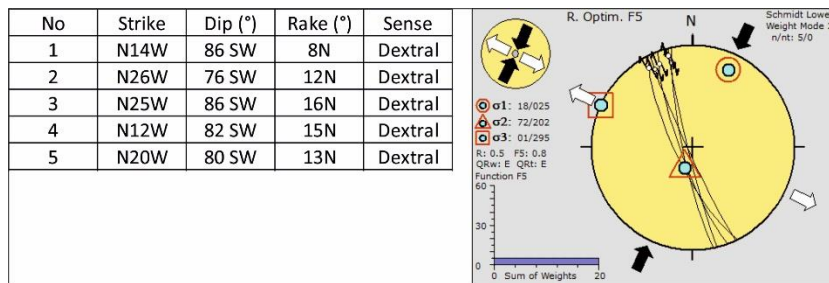


Figure 3-5. Slickenlines measured from Karataş Fault and paleostress reconstruction using Angelier's direct inversion method on Schmidt's lower hemisphere. (White arrow:  $\sigma_3$ ; Grey arrow:  $\sigma_2$ ; Black arrow:  $\sigma_1$ ; Black dot:  $\sigma_1$  vertical; Grey dot:  $\sigma_2$  vertical)

Seismic sections showed that this fault continues along the southern margin through Kavak Stream.

### 3.1.3. Demirtaş Fault

Demirtaş Fault is a 2 km long, steep (77°-85°) sinistral strike-slip fault with a strong normal component that dips towards east. It outcrops near Kızıldere Village with NNE trend and continues along Kavaklı stream with NNE to N-S trend along the northern margin of the Büyük Menderes graben. It cuts and deforms Middle Miocene - Late Miocene Sazak Formation. Similar to the other N-S trending faults, this was also cut and displaced by most of the E-W trending faults; resulting in a change in its trend. Steep fault scarps, sudden changes in slope, deeply incised valleys and slickenlines on fault planes were used to recognize this fault (Figure 3-6).

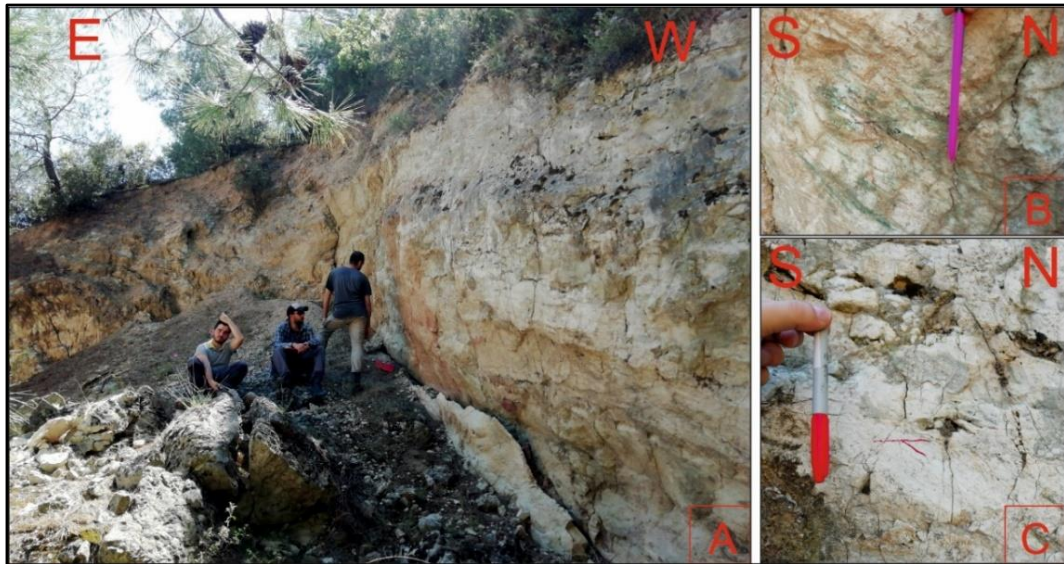


Figure 3-6. A) General view of the surface of Demirtaş Fault; B) and C) Close-up view of slickenlines on Demirtaş Fault on Kavak Valley (see Figure 3-1 for its location).

Paleostress reconstruction showed that Demirtaş Fault is a normal fault with approximately NE-SW extension (Figure 3-7).

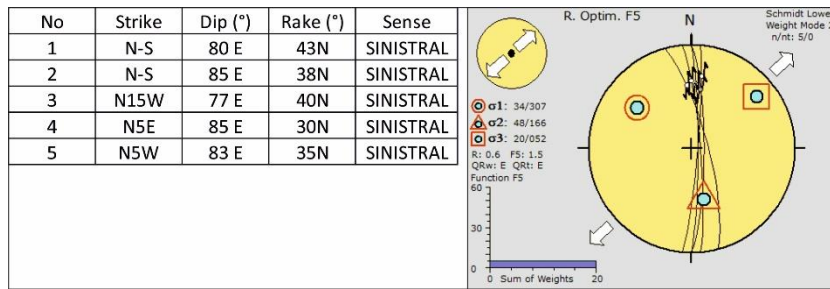


Figure 3-7. Slickenlines measured from Demirtaş Fault and paleostress reconstruction using Angelier's direct inversion method on Schmidt's lower hemisphere. (White arrow:  $\sigma_3$ ; Grey arrow:  $\sigma_2$ ; Black arrow:  $\sigma_1$ ; Black dot:  $\sigma_1$  vertical; Grey dot:  $\sigma_2$  vertical)

### 3.1.4. Pelitliada Fault

Pelitliada Fault is another steep NNE trending fault located in the Kavak Valley. It is a 2 km long, steep ( $80^\circ$ ) normal fault with a small dextral component that dips towards east. Fault outcrops near Kızıldere Village with NNE trend and continue along the western flank of Kavak valley with NNE to N-S trend in the northern margin of the Büyük Menderes graben. This structure is one of the major components of the Kızıldere geothermal field based on two reasons: 1) it cuts and juxtaposes cover and core rocks of Menderes Massif and Miocene rocks; 2) it marks the western edge of paleo basin (Kızılburun and Sazak Formation). Similar to the other N-S trending faults, this was cut and displaced by most of the E-W trending faults; resulting in a change in its trend. Steep fault scarps, sudden changes in slope, deeply incised valleys were used to recognize this fault. Unfortunately, the number of slickenline data is limited to this fault because of extensive deformation on the fault plane. Measured slickenlines indicate that this normal fault has a trend of N15E and dips at  $80^\circ$  with  $75^\circ$  rake to the south (Figure 3-8).

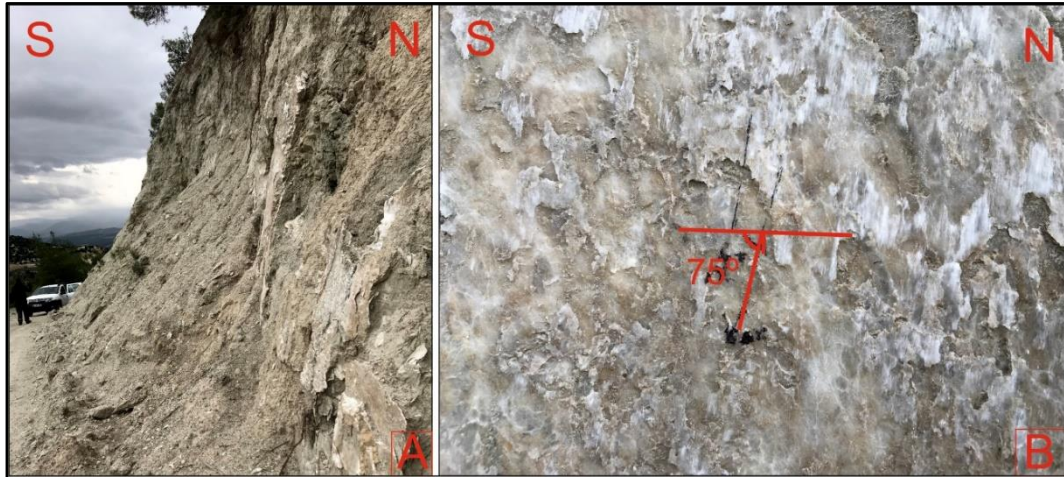


Figure 3-8. A) General view of the surface of Pelitliada Fault; B) Close-up view of slickenlines on Pelitliada Fault on Kavak Valley (see Figure 3-1 for its location).

### 3.1.5. Payamlık Fault

Payamlık Fault is a steep NNE to NNW trending fault located in the Arap Valley along the southern margin of the Büyük Menderes graben. It is a 1.6 km long, steep ( $\sim 80^\circ$ ) normal fault that dips towards east. Fault outcrops well at Arap Valley with NNE trend and continues towards Payamlık Hill with NNW trend. Similar to the other N-S trending faults, this was also cut and displaced by most of the younger E-W trending faults; resulting in a change in its trend. Steep fault scarps, sudden changes in slope, deeply incised valleys were used to recognize this fault (Figure 3-9).



Figure 3-9. General view of Payamlık Fault scarp near Payamlık Hill (see Figure 3-1 for its location).

### 3.1.6. Minor Faults

Other N-S trending faults studied from west to east are shown as Fault A, Fault B, Fault C, Fault D and Fault E on the geological and structural map given as Figure 2-2 and 3-1. These minor structures are generally secondary faults developed as synthetic or antithetic to the main fault.

Fault A, located on the northern margin of the Büyük Menderes graben, is NNE to NNW trending, 1.8 km long steep ( $\sim 75^\circ$ ) normal fault that dips towards east. It cuts and juxtaposes Middle Miocene - Late Miocene Sazak Formation and Late Miocene - Late Pliocene Kolankaya Formation. Although slickenline data is scarce, steep fault scarps, sudden changes in slope, deeply incised valleys were used to recognize this fault. Probably this fault was developed as an antithetic to the Gebeler Fault.

Fault B, located on the northern margin of the Büyük Menderes graben, is another antithetically developed fault to the Gebeler Fault with trend nearly parallel to the Fault A. It is a 2 km steep ( $\sim 75^\circ$ ) normal fault dipping east and deforming Early Miocene - Middle Miocene Kızılburun Formation, Middle Miocene - Late Miocene Sazak Formation and Late Miocene - Late Pliocene Kolankaya Formation. Steep fault scarps, sudden changes in the slope, deformation surfaces, geothermal alteration and sudden changes in slope were commonly observed along the fault zone. It is possible

to track this fault from Hamamaltı to Cankurtaran Hill as a deeply incised narrow valley (Figure 3-10).



Figure 3-10. General view of Fault B surface near Cankurtaran Valley (see Figure 3-1 for its location).

Fault C, located on the northern margin of the Büyük Menderes graben, is a synthetically developed fault to the Gebeler Fault with trend nearly parallel to the Gebeler Fault. It is a 1.6 km steep ( $\sim 70^\circ$ ) normal fault dipping west and deforming Middle Miocene - Late Miocene Sazak Formation and Late Miocene - Late Pliocene Kolankaya Formation. Steep fault scarps, sudden changes in the slope and sudden changes in slope were commonly observed along the fault zone. It is possible to track this fault from İmam Hill and to the east of Cankurtaran Hill as a deeply incised narrow valley.

Fault D located east of Gebeler Valley is a steep ( $\sim 75^\circ$ ) normal fault with NNE to NNW trend that dips towards west. Fault D cuts both Middle Miocene - Late Miocene Sazak Formation and Late Miocene - Late Pliocene Kolankaya Formation. This 2 km

long fault starts from the İmam Hill and continues along as a deeply incised valley towards the north until it fades south of Gökdere Fault. Most probably this structure was developed as a synthetic to the Gebeler fault.

East dipping Fault E was recognized as an antithetic fault of the west-dipping Karataş Fault. Fault E cuts and juxtaposes both Middle Miocene - Late Miocene Sazak Formation and Late Miocene - Late Pliocene Kolankaya Formation. Outcrop of this 2.5 km long fault starts from Karataş Village and continues towards north along Cinlisu Valley. This normal antithetic fault has a dip amount of 85°.

### **3.2. E-W Trending Faults**

In the study area, these faults are E-W and WNW-ESE trending, high angle normal and oblique faults developed under N-S extensional neotectonics. Neotectonic faults consist of set of parallel active faults including the northern and southern margin boundary faults of Büyük Menderes graben. Generally, these faults become younger closer to the margin of the Büyük Menderes graben and they cut and displaced most of the N-S trending faults mentioned in section 3.1. Best criteria to recognize these structures in the field are slickenlines, step-like morphology, steep fault scarps, displacement along streams, sudden changes in slope, deeply incised valleys, fault-controlled alluvial fan deposits, highly deformed and brecciated rocks. Any slickenline data found on the fault planes were measured and photographed.

It is known that active extensional domains and related normal faults are suitable areas for geothermal exploration. In terms of geothermal activity, younger faults are preferred because of their fault sealing behavior since younger faults have lower contents of fault gouge. On the other hand, older faults with their high amount of fault gouge can retard fluid flow.

### 3.2.1. Gökdere Fault

Gökdere fault, which is located on the northern flank of Büyük Menderes graben, has a length of 7.5 km and an E-W to NNW-ESE trend. It is an oblique-slip fault dipping south to southwest with varying amounts. Dips were measured as 60° to the southeast, near Örenli on limestones while in Gebeler Valley it was measured between 40°-50° on metamorphic rocks. This fault starts from Örenli and continues west to the Demirtaş Fault. Towards north-east of Örenli, this fault juxtaposes Kızılburun and Sazak Formations while to the west it juxtaposes metamorphic rocks and paleo formations (Kızılburun and Sazak Formations). Steep fault scarps, displacement along streams, highly deformed and brecciated rocks, sudden changes in slope, deeply incised valleys and well-preserved slickenlines were used to trace Gökdere Fault (Figure 3-11).



Figure 3-11. A) General view of the surface of Gökdere Fault; B) Close-up view of slickenlines on Gökdere Fault; C) Close-up view of brecciated surfaces on Gökdere Fault (see Figure 3-1 for its location).

Paleostress reconstruction of slickenlines obtained from Gökdere Fault showed that it is an oblique-slip fault with approximately N-S extension (Figure 3-12).

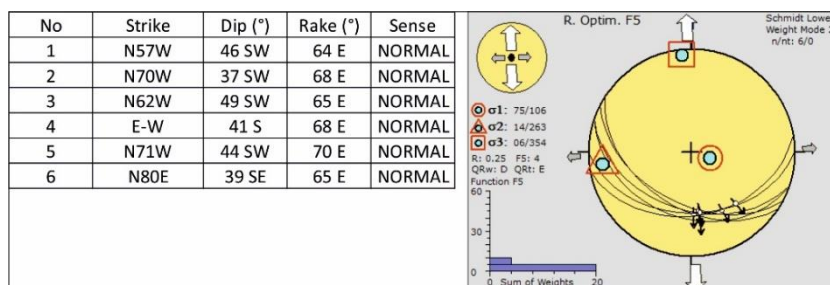


Figure 3-12. Slickenlines measured from Gökdere Fault and paleostress reconstruction using Angelier's direct inversion method on Schmidt's lower hemisphere. (White arrow:  $\sigma_3$ ; Grey arrow:  $\sigma_2$ ; Black arrow:  $\sigma_1$ ; Black dot:  $\sigma_1$  vertical; Grey dot:  $\sigma_2$  vertical)

### 3.2.2. Fault 1

Fault 1 is the youngest fault recognized on the northern flank of the Büyük Menderes graben since it controls the deposition of Quaternary aged Tosunlar Formation. It has a length of 10 km and has an E-W to NNW-ESE trend. This normal fault dips south to the southeast with a dip of 60°-65°. Fault 1 outcrops near İmam Hill and continues along Hamam Mountain and Akyaka in the west. It cut and displaces most of the N-S trending faults in the vertical and lateral direction. This fault juxtaposes Quaternary aged Tosunlar Formation, Kolankaya Formation, and metamorphic rocks. Although the fault plane data could not be found, steep fault scarps, displacement along streams, sudden changes in slope, step-like morphology and fault-controlled alluvial fan deposits were used to trace this fault (Figure 3-13).



Figure 3-13. Panoramic view of the Fault 1 scarp near İmam Mountain (see Figure 3-1 for its location).

### 3.2.3. Fault 2

Fault 2, located on the northern flank of the Büyük Menderes graben, is a 6.5 km long, E-W trending steep normal fault dipping south with  $65^{\circ}$ - $85^{\circ}$ . It starts north of Karataş Village and continues west through Dolomanlı and Hamam Mountains. It surfaces near Maden Stream but the trace of this fault towards the west was lost. It cuts and displaces most of the N-S trending faults in the vertical and lateral direction. This fault juxtaposes Kolankaya Formation and Sazak Formation forming a tectonic boundary between them. Steep fault scarps, displacement along streams, sudden changes in slope, step-like morphology and slickenline were used to recognize this fault (Figure 3-14).



Figure 3-14. A) General view of the Fault 2 scarp; B) Close-up view of slickenlines on Fault 2 along the Cankurtaran Stream (see Figure 3-1 for its location).

Paleostress reconstruction of data obtained from Fault 2 showed that it is a normal fault with approximately N-S extension (Figure 3-15).

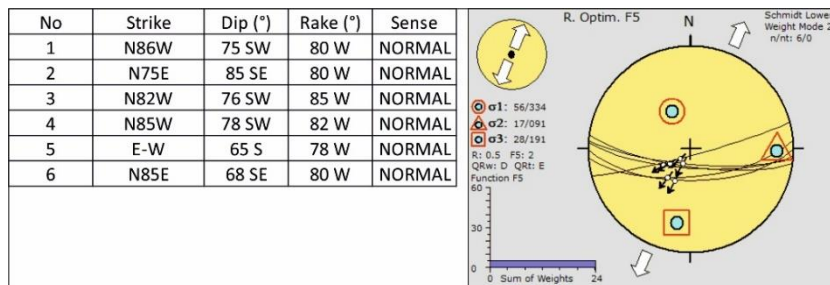


Figure 3-15. Slickenlines measured from Fault 2 and paleostress reconstruction using Angelier's direct inversion method on Schmidt's lower hemisphere. (White arrow:  $\sigma_3$ ; Grey arrow:  $\sigma_2$ ; Black arrow:  $\sigma_1$ ; Black dot:  $\sigma_1$  vertical; Grey dot:  $\sigma_2$  vertical)

### **3.2.4. Fault 3**

It is an 11 km long, E-W to NNW-ESE trending normal fault dipping south to southwest with 60°-80°. It starts from south of Örenli, parallel to Fault 2 and continues towards Kızıldere Village and Old Savcılı. It cuts and displaces most of the N-S trending faults in the vertical direction. Towards the west of Kızıldere Village both metamorphic basement and Tosunlar Formation were cut and juxtaposed. Steep fault scarps, displacement along streams, sudden changes in slope, step-like morphology were used in the recognition of this fault.

### **3.2.5. Fault 4**

It is a 10 km long, E-W to NNW-ESE trending normal fault dipping south to southwest with 60°-78°. Similar to Fault 3 and 2, it starts south of Örenli and continues towards Kızıldere Village and Dela Mountain. It cuts and displaces most of the N-S trending faults in the vertical direction. Near Kızıldere this fault juxtaposes Kolankaya Formation and Sazak Formation. Towards the west of Kızıldere Village metamorphic rocks were deformed. Steep fault scarps, displacement along streams, sudden changes in slope, step-like morphology and slickenlines were used to recognize this fault (Figure 3-16).

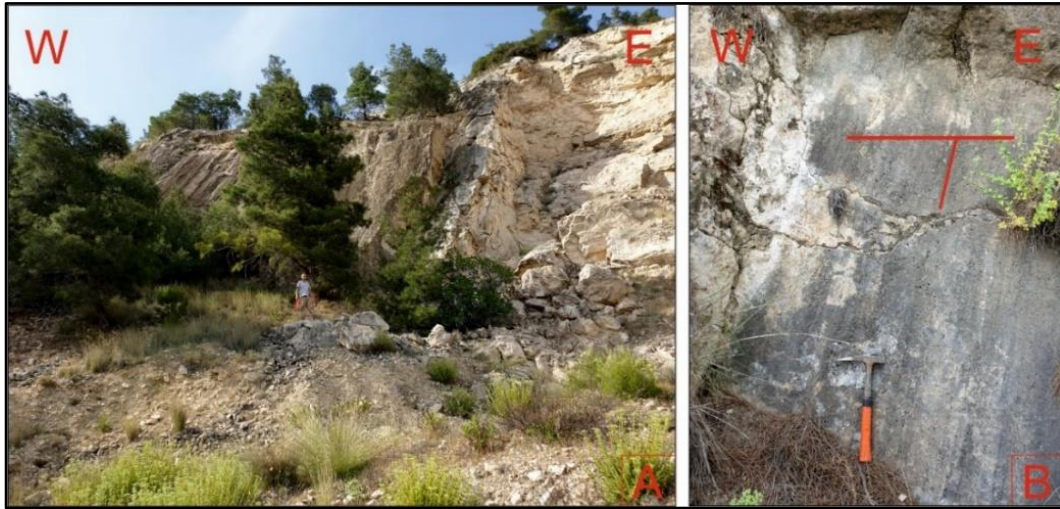


Figure 3-16. A) General view of the surface of Fault 4; B) Close-up view of slickenlines on Fault 4 near Örenli (see Figure 3-1 for its location).

Paleostress reconstruction of data obtained from Fault 4 showed that it is a normal fault with approximately N-S extension (Figure 3-17).

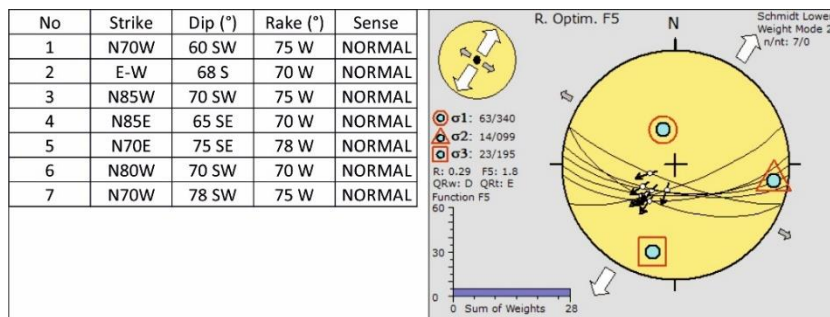


Figure 3-17. Slickenlines measured from Fault 4 and paleostress reconstruction using Angelier's direct inversion method on Schmidt's lower hemisphere. (White arrow:  $\sigma_3$ ; Grey arrow:  $\sigma_2$ ; Black arrow:  $\sigma_1$ ; Black dot:  $\sigma_1$  vertical; Grey dot:  $\sigma_2$  vertical)

### 3.2.6. South Margin Faults

Most of the faults located on the southern margin of the Büyük Menderes graben show similar characteristics to the E-W trending normal faults located on the northern margin. These are usually NW-SE to E-W trending normal faults that dip towards the north. Dip angles range between 65° to 75°. They cut and displace most of the N-S trending fault. Neogene basin in-fill deposited during the neotectonic period were controlled by these faults. Steep fault scarps, displacement along streams, sudden changes in slope, step-like morphology were used to recognize these faults (Figure 3-18). These faults are named as S.F-1, S.F-2 and, S.F-3.



Figure 3-18. Step-like morphology observed in the southern margin of the Büyük Menderes graben (see Figure 3-1 for its location)



## CHAPTER 4

### 3D STRUCTURAL-GEOLOGICAL MODELING

Geothermal exploration requires a good knowledge of the underground geology. This includes caprock-reservoir rock relation, basin analysis and structural network of faults which support the geothermal fluid flow. For this purpose, 3D structural and geological model of the Kızıldere geothermal field was constructed. These models include both field observation (chapter 2 and 3) and well-data. Data from a total of 76 wells were used to design stratigraphic horizons and geometry of faults. Field observations used during geological mapping was the basis for the interpretation of well-data and stratigraphic horizons. Mud losses occurred during drilling could provide some information regarding faults. Both partial mud loss and total loss of drilling mud can occur when the drill bit encounters empty voids in the rock. These voids could be fissures, caverns or fractures. A powerful tool, which can be used to interpret the existence of faults, could be created by combining mud loss values and field observations. In this study, surface expression of faults was correlated with mud losses encountered in wells. Mud loss values in a well could be partial or total where the circulation is completely lost. During the interpretation, faults were assigned to the highest mud loss intervals. On the other hand, for constant high mud loss values faults were appointed to the interval where the first mud loss occurred.

Leapfrog Geothermal, which is 3-D modeling and visualizing software developed by Aranz Geo, was used to create a 3D structural and geological model of the Kızıldere geothermal field. The focus of this model is on major faults described in earlier chapters and important stratigraphic horizons. Tosunlar Formation and overlying recent deposits were not separated since they have little significance in terms of a geothermal system.

### 4.1. 3D Lithological Model

The lithological model was created in two steps: 1) Introducing well-data and creating the first output volumes; 2) Editing these volumes with the geological map to develop a realistic geological model.

#### 4.1.1. Modeling Metamorphic Rocks

In this model cover rocks and core, are separated as metamorphic rocks and gneiss. Field observations and well-data show that metamorphic rocks have two contacts which are Kızılburun Formation and gneiss towards the west of the study area. Depth of metamorphic basement is deepest at the center of graben and towards both margins, basement rocks elevate (Figure 4-1). Metamorphic rocks outcrop towards the north near Gökdere Fault and this model was edited to show this relation. Also, towards east basement depth increases rapidly up to -1750 meter.

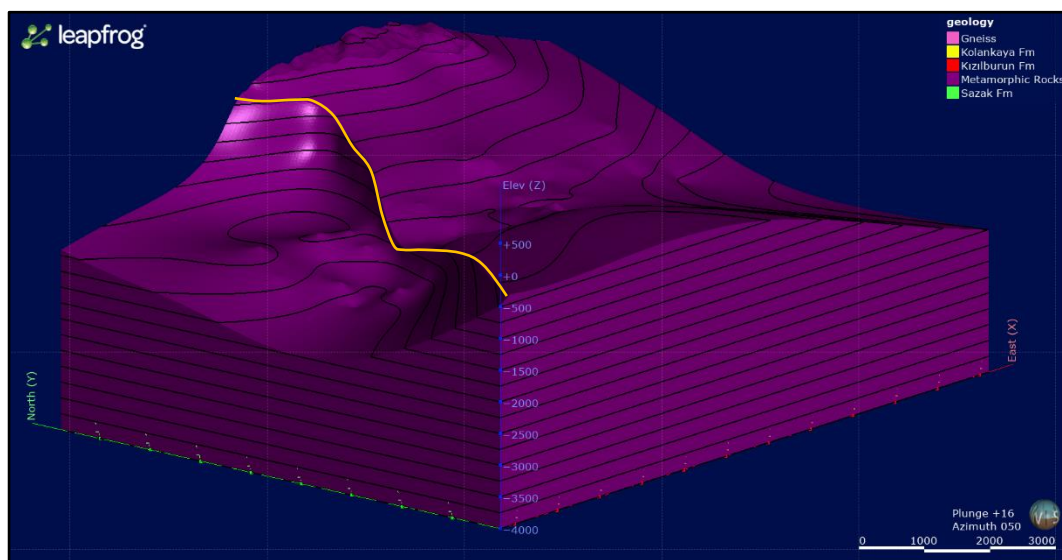


Figure 4-1. The output volume of the metamorphic rocks. (Looking northeast, 250-meter contour spacing). The yellow-colored line is the boundary between gneiss and other metamorphic rocks.

There is a depression towards the west of the model and a sharp boundary surface. Allochthonous gneiss rocks were thrust in this empty area. The boundary was created by using borehole data (yellow-colored line in Figure 4-1).

Gneiss has two overlying contacts which are Kızılburun Formation to the east of the Pelitliada Fault and Kolankaya Formation west of the Pelitliada Fault. These high P/T rocks outcrop at both margin of the graben. The thickness of gneiss increases towards the west of the Pelitliada Fault (Figure 4-2).

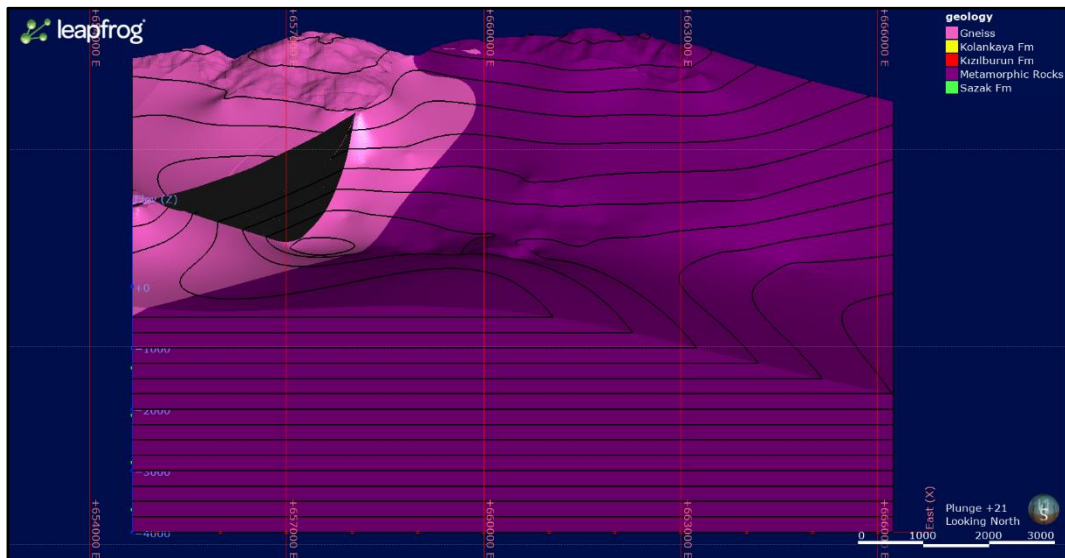


Figure 4-2. The output volumes of metamorphic rocks and gneiss. The black-colored surface represents the Pelitliada Fault. (Looking North, 250-meter contour spacing)

#### 4.1.2. Modeling Kızılburun and Sazak Formations

Field observations showed that the extent of Kızılburun and Sazak Formations are limited in the west. This was also confirmed by well-data (Figure 4-3). There is a sharp N-S trending boundary where the lateral extent of Kızılburun and Sazak Formations are limited. The thickness of these deposits increases towards west until they meet

with this boundary and cease to exist. This boundary mentioned here was indeed the Pelitliada Fault. Both Kızılburun and Sazak Formations onlap to this tectonic surface.

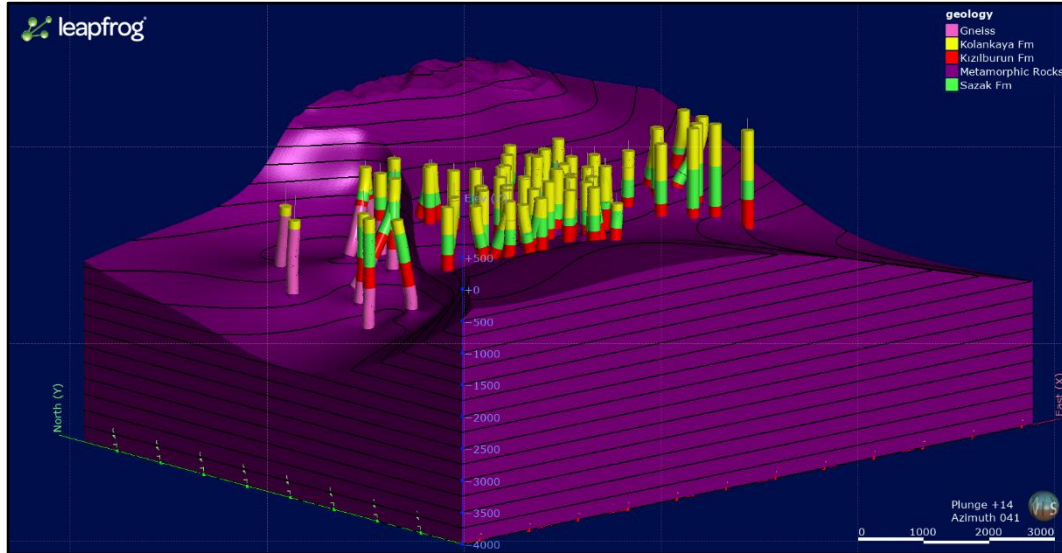


Figure 4-3. Well-data showing the lateral extent of Kızılburun and Sazak Formations. (Looking northeast, 250-meter contour spacing)

Kızılburun Formation outcrops on both northern and southern margin of the Büyük Menderes graben. Depth of this formation increases towards east and southeast (Figure 4-4). As mentioned in section 2 this formation provides good caprock properties. Although it is bounded to the west by Pelitliada Fault this formation covers most of the basement in the eastern part and behaves as a caprock for the reservoirs in metamorphic rocks located to the east of Pelitliada Fault.

Sazak Formation was edited to show exposures both along the northern and southern margin of the Büyük Menderes graben. Similar to the Kızılburun Formation depth of this formation increases towards east and southeast (Figure 4-5). Sazak Formation consists of limestones with karstic nature and forms the second reservoir unit located at the eastern part in this geothermal system.

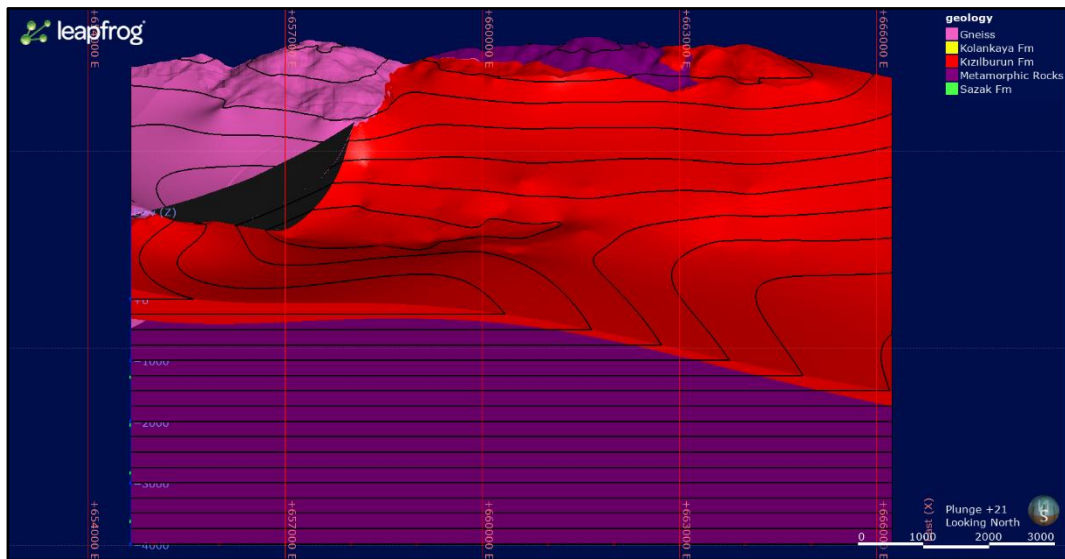


Figure 4-4. The output volume of Kızılburun Formation. The black-colored surface represents the Pelitliada Fault. (Looking north, 250-meter counter spacing)

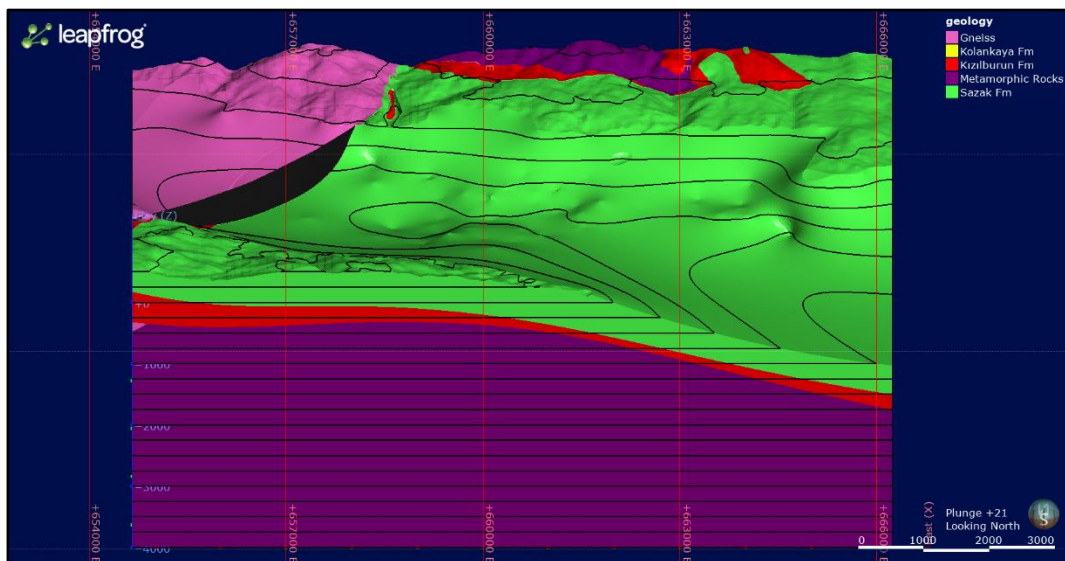


Figure 4-5. The output volume of Sazak Formation. The black-colored surface represents the Pelitliada Fault. (Looking north, 250-meter counter spacing)

### 4.1.3. Modeling Kolankaya Formation

Kolankaya Formation shows full lateral extension along the basin and covers all of the earlier deposits (Figure 4-6). Formation thickens and deepens towards east and southeast. In terms of the geothermal system this region-wide formation provides an excellent caprock for reservoirs in Sazak Formation, metamorphic rocks and gneiss.

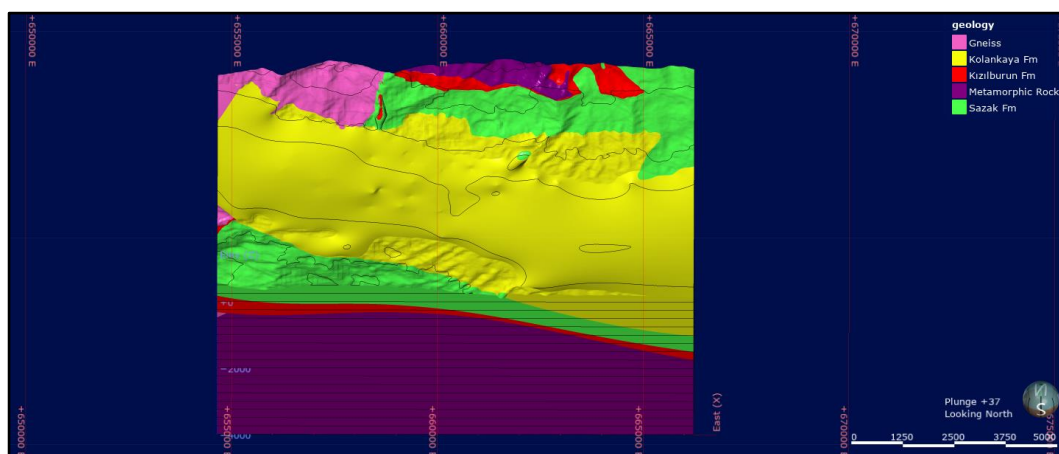


Figure 4-6. The output volume of Kolankaya Formation. (Looking north, 250-meter counter spacing)

In order to understand relation of Kızılburun, Sazak and Kolankaya Formations with Pelitliada Fault a cut-out section was prepared (Figure 4-7). It is clear that this fault was the margin of the paleo basin during deposition of Sazak and Kızılburun Formation. Both of these formations onlap to gneiss and this tectonic surface. Before onlapping the thickness of these deposits reaches their local maximum values. On the other hand, Kolankaya Formation passes through this boundary covering both Sazak Formation on east and gneiss on the west. This shows that Kolankaya Formation deposited in the neotectonic period and there should be an unconformity between paleo basin fill and Kolankaya Formation.

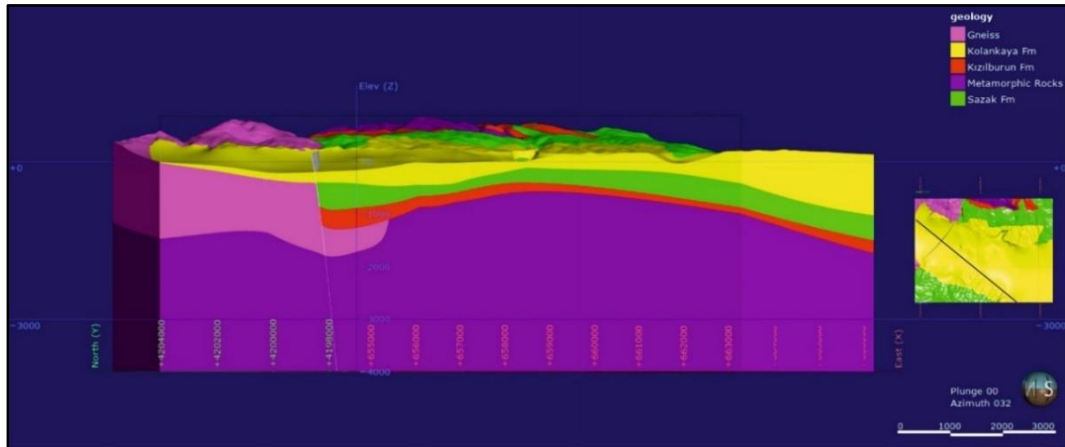


Figure 4-7. Cut-out section showing the onlap surface of older deposits and their stratigraphic relation with Kolankaya Formation. (Looking north-northwest).

#### 4.1.4. Modeling Tosunlar Formation and Recent Deposits

In this 3D model, Tosunlar Formation and recent deposits were not separated and a combined volume of Quaternary Deposits was created. Lithological model both honors surface outcrops of the rocks and well-data. Finalized 3D lithological model of the Kızıldere geothermal field can be seen with different perspectives as in Figure 4-8, 4-9, 4-10 and 4-11.

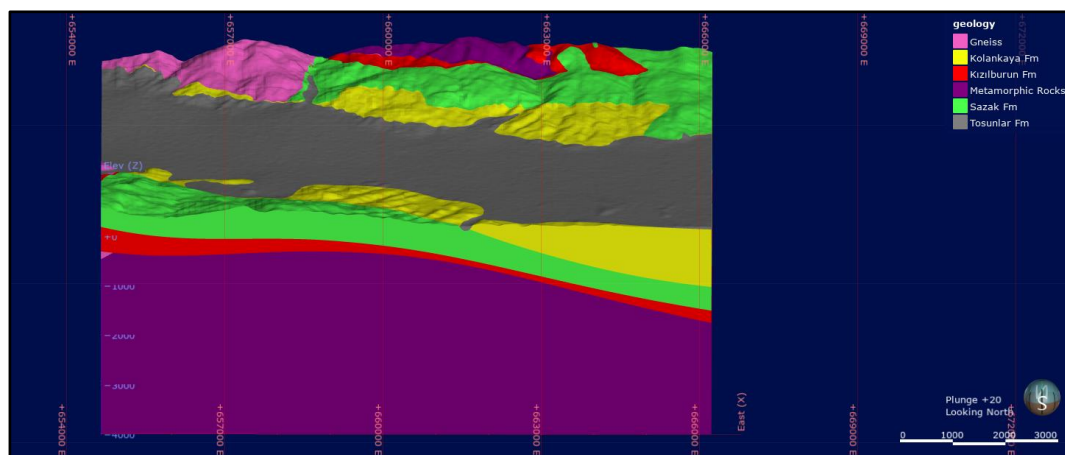


Figure 4-8. Finalized 3D lithological model of the Kızıldere geothermal field. (Looking north)

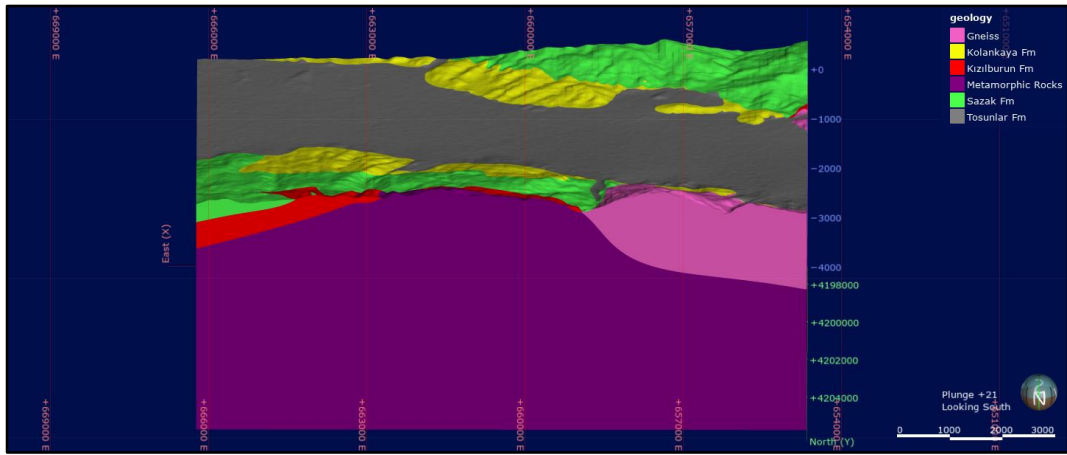


Figure 4-9. Finalized 3D lithological model of the Kızıldere geothermal field. (Looking south)

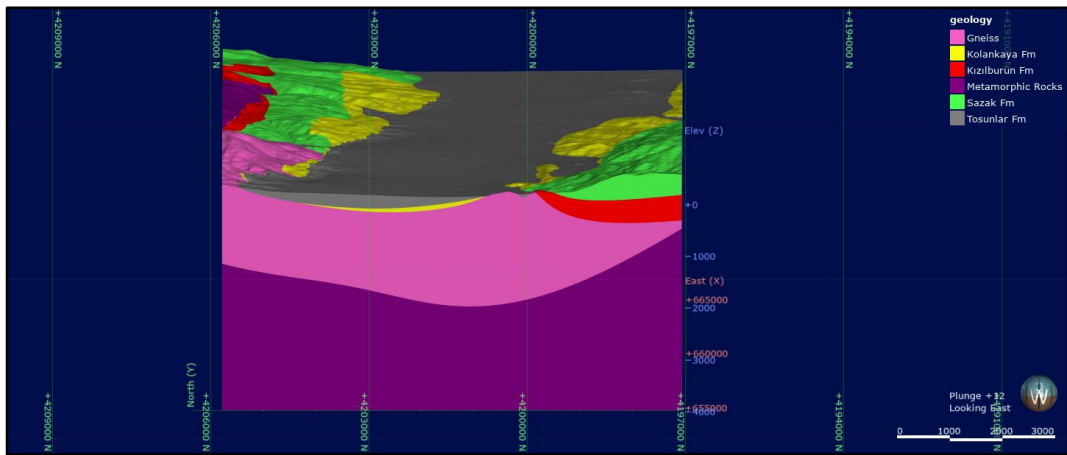


Figure 4-10. Finalized 3D lithological model of the Kızıldere geothermal field. (Looking east)

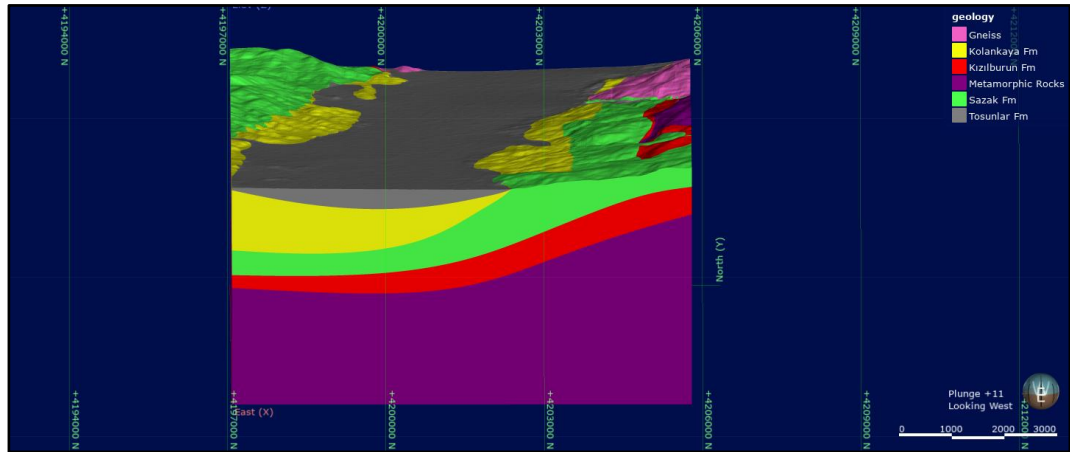


Figure 4-11. Finalized 3D lithological model of the Kızıldere geothermal field. (Looking west)

## 4.2. 3D Structural Model

3D Structural model was created in two steps: 1) Forming fault planes with field observations; 2) Editing fault surfaces with well-data by using drilling mud loss intervals as an indicator of faults. The maximum snap distance was set to 100 meters. Data outside of this distance was not used in order to minimize errors and get better results.

### 4.2.1. E-W Trending Faults

Modeled fault planes include Fault 1, Fault 2, Fault 3, Fault 4 and Gökdere Fault located at the northern margin of the Büyük Menderes graben. In addition, three fault planes located at the southern margin were modeled: SF-1, 2 and 3.

Fault 1 surface was generated using the trace of fault in the geological map. The dips of the faults were assigned according to field data. There are a bunch of wells with mud loss intervals to edit this faults underground geometry (Figure 4-12). Field observations showed that Fault 2 disappears towards the west after Maden Stream and for this reason in this model this fault terminates against Fault 1.

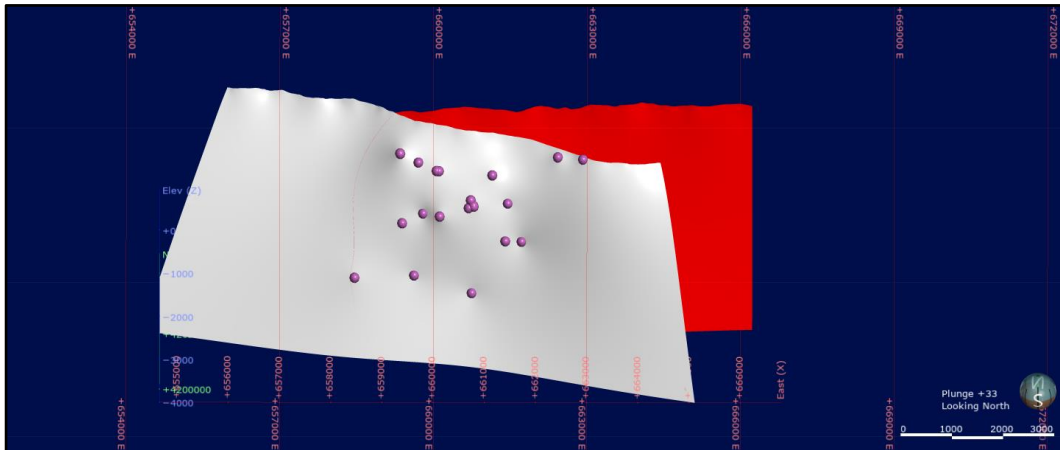


Figure 4-12. Modeled fault planes of Fault 1 (white-colored surface) and Fault 2 (red-colored surface). Pink colored dots are mud loss intervals encountered in Fault 1 that was used to edit the surface of the fault. (Looking north)

Remaining E-W trending faults located on the northern margin of Büyük Menderes graben were generated with the same principles (Figure 4-14).

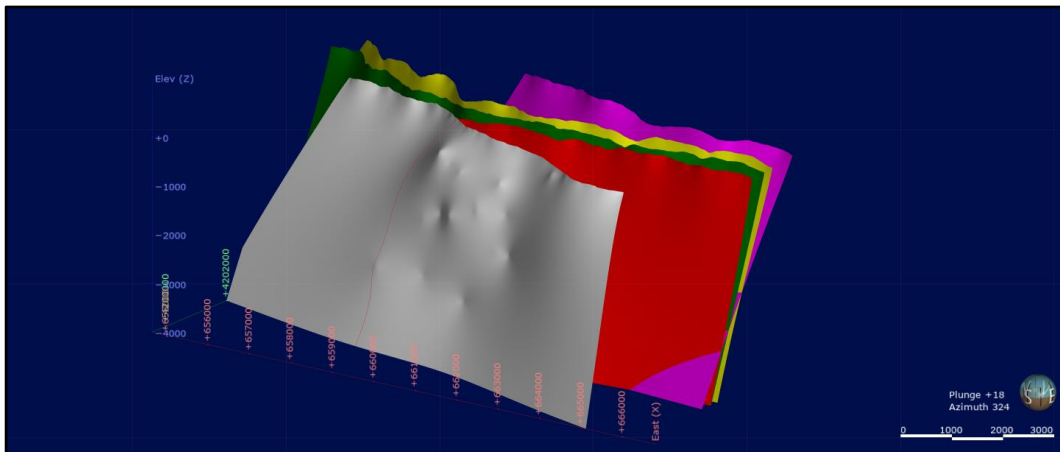


Figure 4-13. Modeled fault planes along the northern margin of the Büyük Menderes graben (White-colored surface: Fault 1; Red-colored surface: Fault 2; Green-colored surface: Fault 3; Yellow-colored surface: Fault 4; Pink-colored surface: Gökdere Fault). (Looking northwest)

Field studies showed that in the south flank of the Büyük Menderes graben SF-1 terminates against SF-3 near Çatal Hill. In addition, the trace of SF-2 was lost at Hamam Hill but probably this fault continues towards the west as buried. Therefore, in the structural model surface of these faults terminates against SF-3 (Figure 4-14).

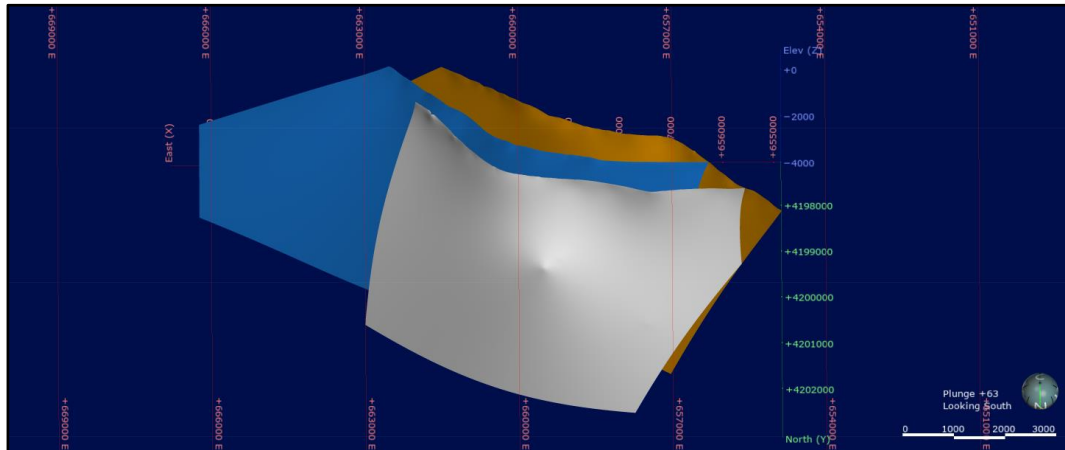


Figure 4-14. Modeled fault planes along the southern margin of the Büyük Menderes graben (White-colored surface: SF-1; Blue-colored surface: SF-2; Orange-colored surface: SF-3). (Looking southeast)

Obtained data is not enough to determine what occurs in the intersection of southern and northern margin faults. For this reason, in the model, these faults were modeled to cross over. Structural model of E-W trending faults both along the northern and southern margin of the Büyük Menderes graben can be seen as in Figure 4-15.

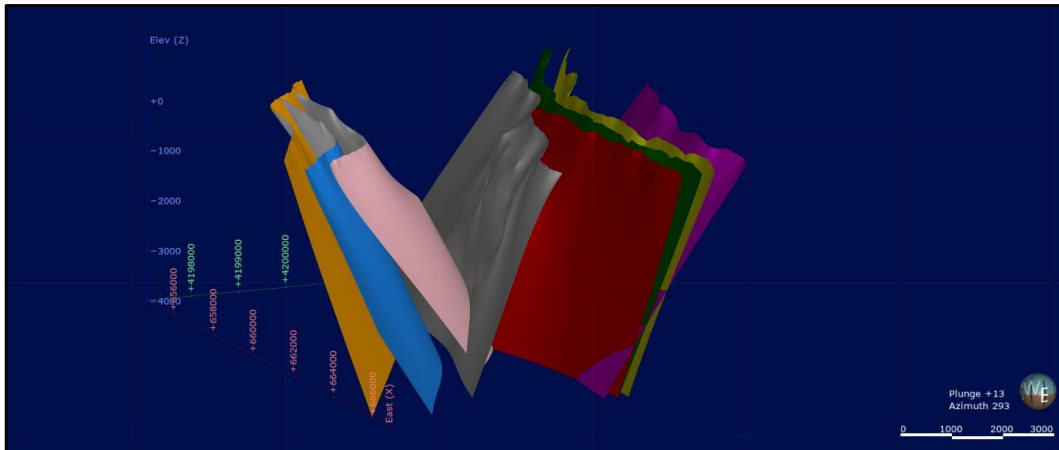


Figure 4-15. Structural model of E-W trending normal faults. (Looking west)

#### 4.2.2. N-S Trending Faults

Same principles were used in modeling N-S trending faults. One of the main structures in the Kızıldere geothermal field is the Gebeler Fault Zone. This zone consists of the main fault, which is Gebeler Fault itself, and other minor synthetics/antithetic faults. The model was created in a way that these antithetic (Fault A, B) and synthetic (Fault C, D) structures terminate against the Gebeler Fault (Figure 4-16). Although displacements were observed at the intersections of E-W trending normal faults and N-S trending faults, reflecting this to the model was impossible based on the available data.

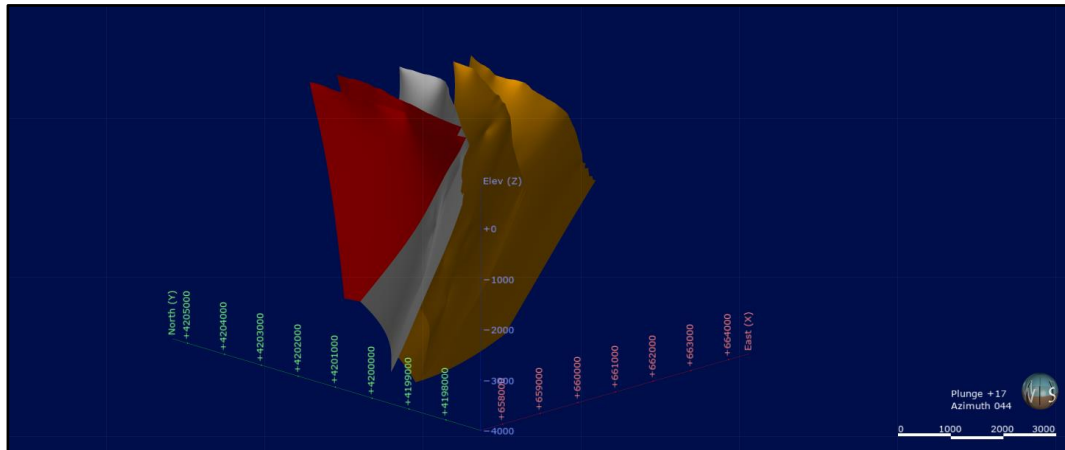


Figure 4-16. Structural modeling of Gebeler Fault Zone (Red-colored surfaces: Antithetic Fault A and B; Orange-colored surfaces: Synthetic Fault C and D; White-colored surface: Main Fault-Gebeler Fault). (Looking North)

Other major N-S trending fault surfaces were also created by first using surface traces of faults and later editing with borehole data (Figure 4-17).

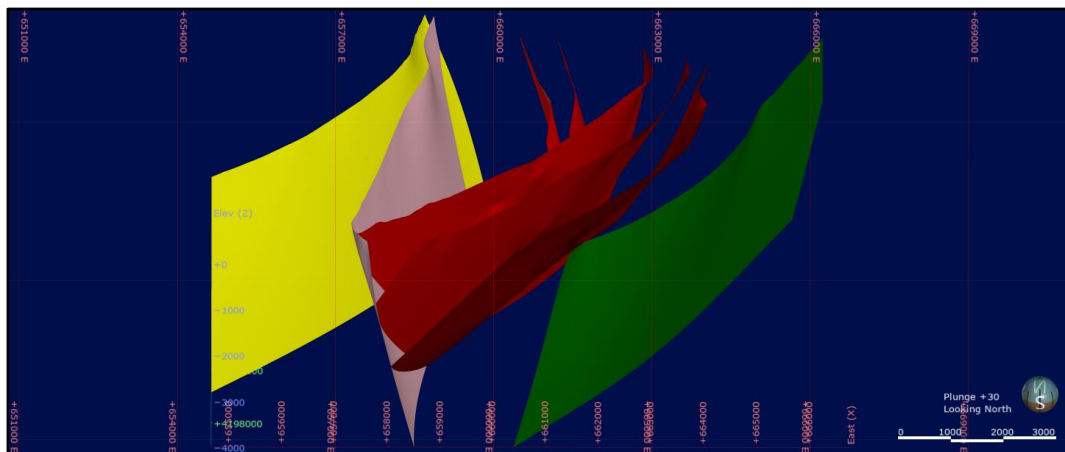


Figure 4-17. Structural model of N-S trending faults. (Red-colored surfaces: Gebeler Fault Zone; Green-colored surface: Karataş Fault; Pink-colored surface: Demirtaş Fault; Yellow-colored surface: Pelitliada Fault). (Looking north)

A cross-section nearly perpendicular to the N-S trending faults was prepared (Figure 4-18). In this section, an offset along gneiss was observed. This shows that there is an 800-meter offset along Pelitliada Fault. In addition, along the Gebeler Fault Zone basement rocks and Kızılburun Formations were elevated which indicates a structural high in this fault zone.

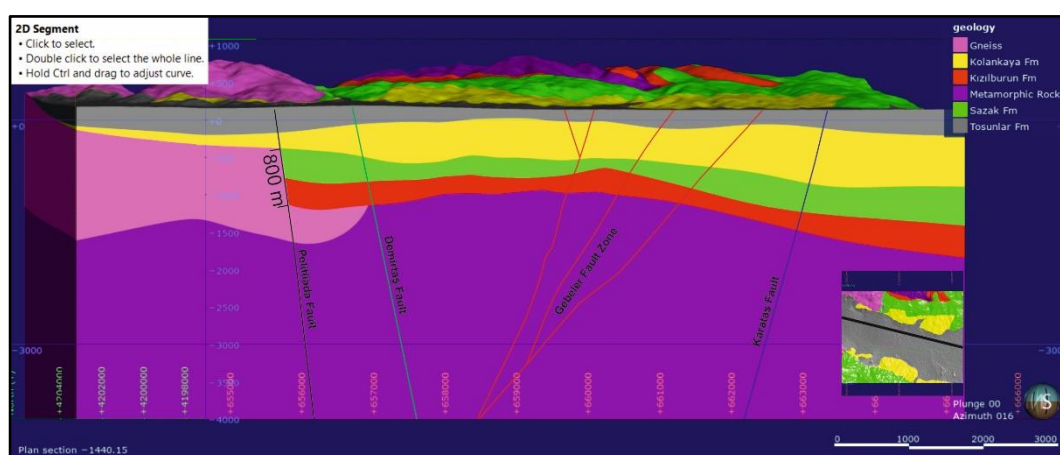


Figure 4-18. Cross-section showing major N-S trending faults. 800-meter offset was calculated along Pelitliada Fault (Black-colored line: Pelitliada Fault; Green-colored line: Demirtaş Fault; Red-colored lines: Gebeler Fault Zone; Blue-colored line: Karataş Fault). (Looking North)

Final 3D structural model governing all of the faults that were modeled can be observed as in Figure 4-19. These are not all of the faults existing in the area. Criteria for choosing these faults are based on their significance on the structural control of the Kızıldere geothermal field.

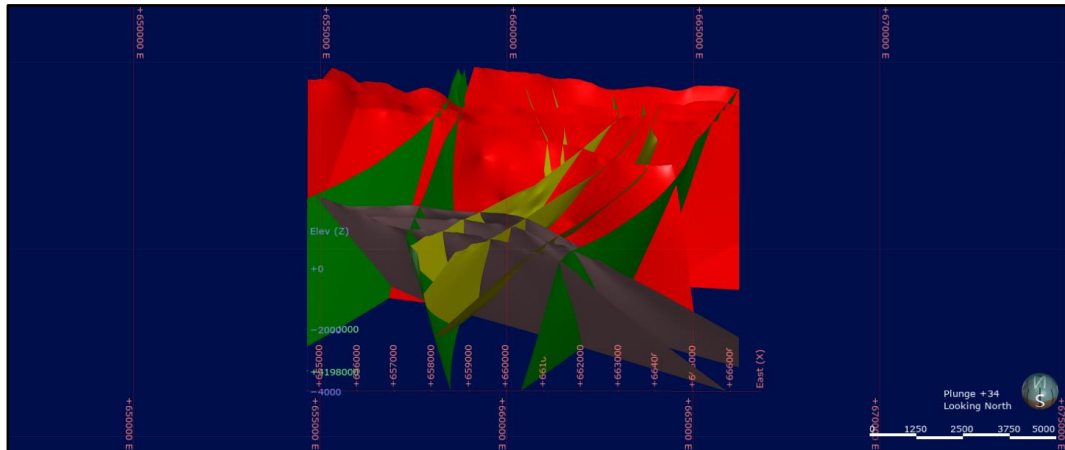


Figure 4-19. Final 3D structural model of the Kızıldere geothermal field (Red-colored surfaces: E-W trending normal faults along the northern margin of the Büyük Menderes graben; Grey-colored surfaces: E-W trending normal faults along the southern margin of the Büyük Menderes graben; Yellow-colored surfaces: Gebeler Fault Zone; Green-colored surfaces: Other N-S trending faults). (Looking north)

### 4.3. 3D Thermal Model

One of the perks of drilling data is reservoir tests which include static formation temperatures. Visualizing temperature distribution along the Kızıldere geothermal field could help to determine which faults are favorable for geothermal exploration. For this purpose, the 3D thermal model of the Kızıldere geothermal field was prepared (Figure 4-20). The extent of this model was constrained with well-data (figure 2-2). The thermal model showed that temperatures higher than 200 °C are located to the west and in the central part of the field. In other words, temperature values drop in the eastern part of the field while higher temperature values are elevated in the central part. To summarize, in terms of thermal distribution central part of the field is the hottest while the eastern part is the coldest and western part is the moderate temperature region.

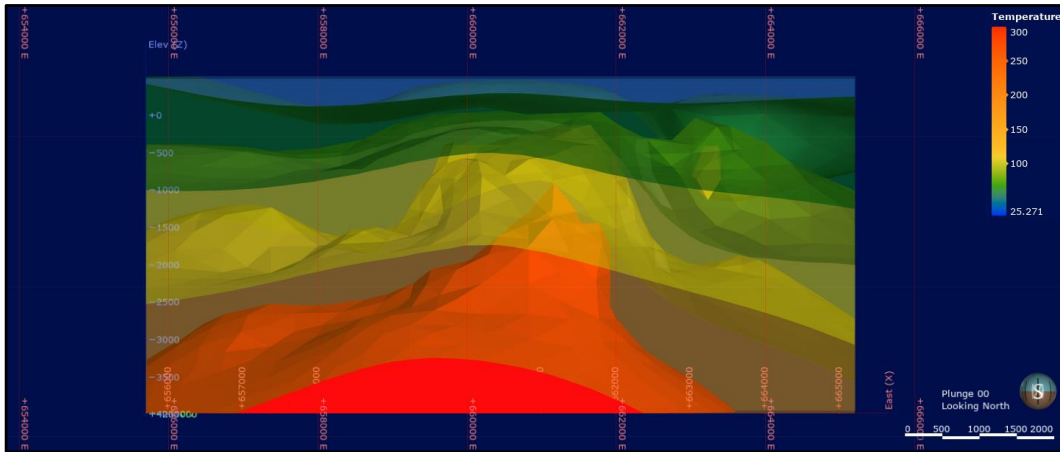


Figure 4-20. Thermal distribution of the Kızıldere geothermal field.

Matching the thermal model with structural model could be useful to understand structural control of the system and point out favorable faults for geothermal exploration. E-W directional cross-section from the highest temperature region was prepared (Figure 4-22). According to this section, temperature values elevate along Gebeler Fault Zone while the geothermal system starts to cool with Karataş, Demirtaş and Pelitliada faults.

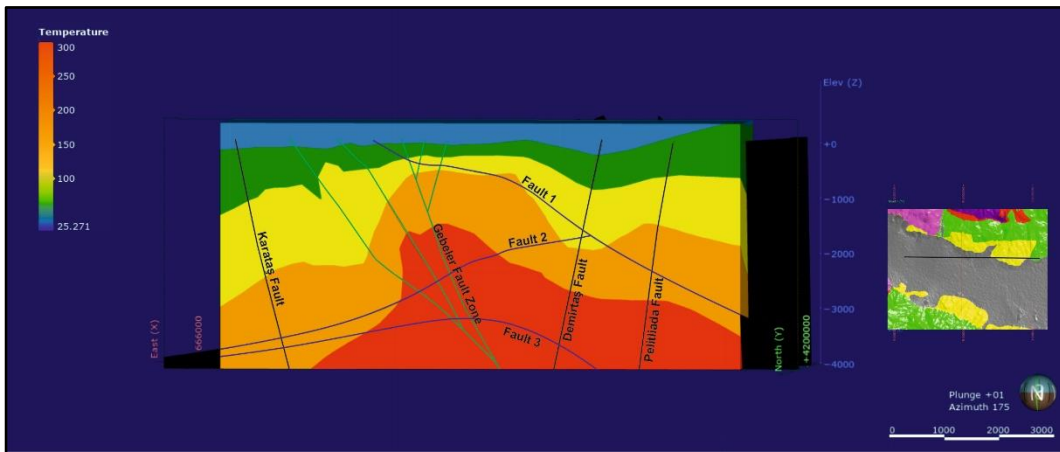


Figure 4-21. E-W cross-section of the thermal and structural model of the Kızıldere geothermal field (Green-colored surfaces: Gebeler Fault Zone; Black-colored surfaces: From east to west Karataş, Demirtaş and Pelitliada faults; Navy blue-colored surfaces: E-W trending faults). (Looking south)

To conclude the highest temperature areas in the Kızıldere geothermal fields can be characterized as the intersection of E-W trending normal faults and N-S trending Gebeler Fault Zone. These faults are the main structures that control the flow of hot geothermal fluids.



## CHAPTER 5

### DISCUSSIONS

All of the components required to develop a geothermal system is present in the Kızıldere geothermal field. Even though it is still debated the source of heat is the result of elevated asthenosphere by ongoing extension in western Anatolia (Kaya, 2015; Koçyiğit, 2015; Roche et al. 2015, 2016, 2018; Gessner et al. 2017). Field studies and 3D models showed that Sazak Formation, which forms the first reservoir is used widely by geothermal fluids. This is evidenced by a number of fumaroles, geothermal alteration surfaces and hot springs found on limestone outcrops of Sazak Formation (Figure 2-2, 2-12). The second reservoir of the system is the metamorphic rocks of Menderes Massif with brittle characteristics such as marble, gneiss, quartzite, quartzschist. High P/T core rocks such as gneiss and low P/T cover rocks of Menderes Massif were found side by side in the study area. Borehole data showed that these core rocks (gneiss) are allochthonous tectonic slices that thrust over cover rocks of Menderes Massif. Apart from that correlation along cover rocks are almost impossible. For this reason, Menderes Massif should be viewed as a package containing different tectonic slices. Kızılburun and Kolankaya Formation can be appointed as the caprock of the system. Sazak Formation rests conformably on the Kızılburun Formation and together they constitute the paleo basin deposits. The western boundary of the paleo basin is the N-S trending Pelitliada Fault where Kızılburun and Sazak Formation onlap on this surface. For this reason, Kızılburun Formation should be viewed as a local caprock. On the other hand, Kolankaya Formation passes this barrier and covers all of the older rocks in the region. This shows that there should be an unconformity surface between paleo basin deposits (Kızılburun and Sazak Formation) and recent basin deposits (Kolankaya and Tosunlar Formation).

During field studies, enough fault plane data were acquired from primary faults. Paleostress reconstructions showed two dominant trends operating in the field. First, E-W trending active graben margin boundary faults, which developed from neotectonic N-S extension, consisting of a set of parallel high angle, normal faults that dip towards the Büyük Menderes graben. The second dominant structures are nearly N-S trending sub-vertical oblique normal and strike-slip faults. These structures are transverse to the neotectonic graben and most of them can be correlated in both margins of the Büyük Menderes graben. Generally, these transverse structures were cut and displaced by the E-W trending normal faults. One of the main structures that control geothermal activity is the N-S directed Gebeler Fault Zone. The activity of this fault zone is evidenced by a number of fumaroles, hot springs and geothermal surface alterations located on it. In addition, the hottest region on the Kızıldere geothermal field was found on Gebeler Fault Zone. Most of the N-S trending faults including Gebeler Fault cut and displace Late Miocene - Late Pliocene aged Kolankaya Formation, meaning they were active until Late Pliocene. On the other hand, Pelitliada Fault as seen in Figure 4-18 was not active during the deposition of Kolankaya Formation and it should be separated from other N-S trending faults. This could be the reason why temperature is lower in this region.

Most of the N-S trending faults, excluding Pelitliada Fault, are transfer faults that developed in extensional tectonics. These accommodation faults link E-W trending normal faults with different displacements. In addition, reactivation surfaces found on these transfer faults gives further evidence that indeed these are transfer faults that connect normal faults with different displacements. These nearly vertical faults cut both the basement and basin fill and act as a conduit for geothermal fluid circulation. Since these structures also cut by other E-W trending normal faults, geothermal fluids are shared with both of them. In addition, there is a N-S trending transverse drainage system located on these faults. Büyük Menderes graben is located between Buldan Horst at the north and Babadağ Horst at the south. Rainfall and melted snow originated from these elevated areas recharge the geothermal system. Meteoric waters first

contact with the system occurs along with these transverse drainage systems. In other words, these deformed fault zones act as channels and permit the discharge of meteoric water into the system while elevating hot geothermal fluids. This should be the reason why geothermal activity and high-temperature values are centered around Gebeler Transfer Fault Zone.

In this study, the importance of N-S trending structures is confirmed with 3D structural and thermal models. Hottest region of the Kızıldere geothermal field is located at the intersection of Gebeler Fault Zone and shear zones of E-W trending normal faults situated in the northern margin of the Büyük Menderes graben. Gebeler Fault Zone consists of a major transfer fault and minor antithetic/synthetic structures creating highly fractured reservoir rocks. Additionally, these transfer faults have a deeper root to carry hot geothermal fluids to the surface. Indeed, faults control the geothermal systems in extensional domains by both managing fluid flow and developing reservoir rocks through creating secondary permeability with brittle deformation. The intersection of E-W trending normal faults and N-S trending strike-slip and oblique faults generates local high permeability reservoir zones. According to the thermal model, zones situated outside of this highly fractured zone is characterized as a cold area.

Apart from Gebeler Fault Zone, N-S trending Pelitliada Fault is also an important structure both for the development of the basin and for this geothermal system. This huge normal fault with approximately measured 800 m vertical offset constitutes the western boundary of the paleo basin. Perhaps it is best to limit the Kızıldere geothermal field with this structure as well since two formations that have an important role in the system are missing in the western part.

A good exploration strategy should comprehend “which structures control the geothermal system”. Interpretations of these models showed Kızıldere geothermal field is mainly controlled by N-S trending transfer faults. In terms of geothermal exploration, a favorable spot for drilling on Kızıldere and similar geothermal fields

located in south-western Anatolia should be along the intersection of parallel E-W trending graben margin boundary faults and transfer faults that dissect the system transversely. Along these critically stressed regions fluid channels would be open (Faulds and Hinz, 2015). Aside from these main structures, Pelitliada Fault which acts as a natural boundary of the geothermal system should be defined for successful exploration and reinjection strategy.

## CHAPTER 6

### CONCLUSION

Geothermal exploration in extensional type domains requires a good understanding of the structural controls. In these systems faults play a major role by controlling the movement of geothermal fluids and distribution of reservoir rocks. Aim of this study is to reveal structural control of the Kızıldere geothermal field, which is one of the hottest fields located in south-western Anatolia. This task requires knowledge on a range of subjects including basin evolution, tectonics, structural geology, and stratigraphy. Creating a geological map is part of this study that enables comprehension of the relations between caprock and reservoir rock. Paleostress calculations of fault plane data such as trend, dip, and rake prove useful in characterizing fault and discovering extension directions.

Borehole data is a precise tool in developing 3D lithological, structural and thermal models. These models showed that hottest regions around the Kızıldere geothermal field are the intersections of N-S trending transfer faults and E-W trending normal margin boundary graben faults. Both static temperature values obtained from wells and geothermal manifestations observed in the field agrees with this type of play concept. Subvertical N-S trending transfer faults with deep roots carry hot geothermal fluids upward while their own drainage system allows the system to recharge with cold meteoric waters. In addition, E-W trending normal faults that cut these transfer faults enhances the fluid flow even further. These highly fractured intersection zones are the main structures controlling the field and favorite spots for the Kızıldere geothermal field and other similar geothermal fields in western Anatolia.



## REFERENCES

- Alçıçek, H. (2007). Denizli Havzası (Denizli-Buldan Bölgesi, GB Türkiye) Neojen Çökellerinin Sedimantolojik İncelemesi [Sedimentological Investigation of Neogene Deposits in Denizli Basin (Denizli-Buldan Region, SW Turkey)] (PhD thesis). Ankara University, Geological Engineering Department, p. 308.
- Alçıçek, H., Varol, B., & Özkul, M. (2007). Sedimentary facies, depositional environments and palaeogeographic evolution of the Neogene Denizli Basin, SW Anatolia, Turkey. *Sedimentary Geology*, 202(4), 596–637. doi:10.1016/j.sedgeo.2007.06.002
- Alçıçek, H., Bülbül, A., Brogi, A., Liotta, D., Ruggieri, G., Capezzuoli, E., ... Alçıçek, M. C. (2018). Origin, evolution and geothermometry of the thermal waters in the Gölemezli Geothermal Field, Denizli Basin (SW Anatolia, Turkey). *Journal of Volcanology and Geothermal Research*, 349, 1–30. doi:10.1016/j.jvolgeores.2017.07.021
- Armijo R., Meyer B., Hubert A., Barka A. (1999). Westward propagation of the North Anatolian fault into the northern Aegean: Timing and kinematics, *Geology*, 27(3),267–270.doi:10.1130/0091-7613(1999)027<0267:WPOTNA>2.3.CO;2
- Barka, A. A., & Kadinsky-Cade, K. (1988). Strike-slip fault geometry in Turkey and its influence on earthquake activity. *Tectonics*, 7(3), 663–684. doi:10.1029/tc007i003p00663
- Barka A. A., (1992). The North Anatolian fault zone, *Ann. Tectonicae*, 6, 164–195.
- Boray A. (1982). Selimiye-Beşparmak yöresindeki (Muğla) Menderes Masifi kayalarının stratigrafisi: tartışma ve Yanıt. *Türkiye Jeoloji Kurumu Bülteni*, 25, 161–162.

- Bozkurt, E., & Park, L. R. G. (1994). Southern Menderes Massif: an incipient metamorphic core complex in western Anatolia, Turkey. *Journal of the Geological Society*, 151(2), 213–216. doi:10.1144/gsjgs.151.2.0213
- Bozkurt, E. (2000). Timing of Extension on the Büyük Menderes Graben, Western Turkey, and Its Tectonic Implications. Geological Society, London, Special Publications, 173(1), 385–403. doi:10.1144/gsl.sp.2000.173.01.18
- Bozkurt, E., & Mittweide, S. K. (2001). Introduction to the Geology of Turkey—A Synthesis. *International Geology Review*, 43(7), 578–594. doi:10.1080/00206810109465034
- Bozkurt, E., & Oberhänsli, R. (2001). Menderes Massif (Western Turkey): structural, metamorphic and magmatic evolution - a synthesis. *International Journal of Earth Sciences*, 89(4), 679–708. doi:10.1007/s005310000173
- Bozkurt, E., Yusufoglu, H., Seyitoğlu, G., Çemen, I., & Tekeli, O. (2002). Discussion on the extensional folding in the Alaşehir (Gediz) Graben, western Turkey. *Journal of the Geological Society*, 159(1), 105–109. doi:10.1144/0016-764901-047
- Bozkurt, E., & Sözbilir, H. (2004). Tectonic evolution of the Gediz Graben: field evidence for an episodic, two-stage extension in western Turkey. *Geological Magazine*, 141(1), 63–79. doi:10.1017/s0016756803008379
- Bozkurt, E., & Rojay, B. (2005). Episodic, two-stage Neogene extension and short-term intervening compression in Western Turkey: field evidence from the Kiraz Basin and Bozdağ Horst. *Geodinamica Acta*, 18(3-4), 299–316. doi:10.3166/ga.18.299-316
- Burchfiel, B. C., Nakov, R., & Tzankov, T. (2003). Evidence from the Mesta half-graben, SW Bulgaria, for the Late Eocene beginning of Aegean extension in the Central Balkan Peninsula. *Tectonophysics*, 375(1-4), 61–76. doi:10.1016/j.tecto.2003.09.001

- Burchfiel, B. C., Nakov, R., Dumurdzanov, N., Papanikolaou, D., Tzankov, T., Serafimovski, T., ... Nurce, B. (2008). Evolution and dynamics of the Cenozoic tectonics of the South Balkan extensional system. *Geosphere*, 4(6), 919. doi:10.1130/ges00169.1
- Bülbül A., Özen T., Tarcan G. (2011). Hydrogeochemical and hydrogeological investigations of thermal waters in the Alasehir-Kavaklidere area (Manisa-Turkey). *African Journal of Biotechnology*, 10(75). doi:10.5897/ajb11.3050
- Candan O., Dora O., Oberhänsli R., Çetinkaplan M., Partzsch J., Warkus F., and Dürr S. (2001). Pan-African high-pressure metamorphism in the Precambrian basement of the Menderes Massif, western Anatolia, Turkey. *International Journal of Earth Sciences*, 89(4), 793–811. doi:10.1007/s005310000097
- Candan, O., Koralay, O. E., Akal, C., Kaya, O., Oberhänsli, R., Dora, O. Ö., ... Chen, F. (2011). Supra-Pan-African unconformity between core and cover series of the Menderes Massif/Turkey and its geological implications. *Precambrian Research*, 184(1-4), 1–23. doi: 10.1016/j.precamres.2010.09.010.
- Çifçi, G., Pamukçu, O., Çoruh, C., Çopur, S., & Sözbilir, H. (2010). Shallow and Deep Structure of a Supradetachment Basin Based on Geological, Conventional Deep Seismic Reflection Sections and Gravity Data in the Büyük Menderes Graben, Western Anatolia. *Surveys in Geophysics*, 32(3), 271–290. doi:10.1007/s10712-010-9109-8
- Cohen, H. A., Dart, C. J., Akyüz, H. S., & Barka, A. (1995). Syn-rift sedimentation and structural development of the Gediz and Büyük Menderes graben, western Turkey. *Journal of the Geological Society*, 152(4), 629–638. doi:10.1144/gsjgs.152.4.0629
- Delvaux, D. and Sperner, B. (2003). Stress tensor inversion from fault kinematic indicators and focal mechanism data: the TENSOR program. In: *New Insights into Structural Interpretation and Modelling* (D. Nieuwland Ed.). Geological Society, London, Special Publications, 212: 75-100.

- Dewey, J.F., Şengör, A.M.C., (1979). Aegean and surrounding regions complex multiplate and continuum tectonics in a convergent zone: Geological Society of America Bulletin, 90,8492.  
doi:10.1130/00167606(1979)90<84:aasrcm>2.0.co;2
- Dewey, J. F. (1988). Extensional collapse of orogens. *Tectonics*, 7(6), 1123–1139.  
doi:10.1029/tc007i006p01123
- Dewey, J. F., Helman, M. L., Knott, S. D., Turco, E., & Hutton, D. H. W. (1989). Kinematics of the western Mediterranean. Geological Society, London, Special Publications, 45(1), 265–283. doi:10.1144/gsl.sp.1989.045.01.15
- Erdoğan, B., Güngör, T. (2004). The problem of the core-cover boundary of the Menderes Massif and an emplacement mechanism for regionally extensive gneissic granites, Western Anatolia (Turkey), *Turk. J. Earth Sci.*, 13, 15–36.
- Erkan, K. (2014). Crustal heat flow measurements in western Anatolia from borehole equilibrium temperatures. *Solid Earth Discussions*, 6(1), 403–426.  
doi:10.5194/sed-6-403-2014
- Erkan, K. (2015). Geothermal investigations in western Anatolia using equilibrium temperatures from shallow boreholes. *Solid Earth*, 6(1), 103–113.  
doi:10.5194/se-6-103-2015
- Faulds, J.E., Bouchot, V., Moeck, I., and Oğuz, K. (2009). Structural controls of geothermal systems in western Turkey: A preliminary report, *Geothermal Resources Council Transactions*, 33, (2009), 375-382.
- Faulds, J. E., & Hinz, N. H. (2015). Favorable Tectonic and Structural Settings of Geothermal Systems in the Great Basin Region, Western USA: Proxies for Discovering Blind Geothermal Systems. *Proceedings World Geothermal Congress 2015 Melbourne, Australia*.
- Filiz S, Tarcan G, Gemici U (2000). Geochemistry of the Germencik geothermal fields, Turkey. *Proceedings of the world geothermal congress*, pp 1115–1120.

- Gessner, K., Ring, U. and Güngör T. (2011). Field Guide to Samos and the Menderes Massif: Along-Strike Variations in the Mediterranean Tethyan Orogen. doi:10.1130/9780813700236
- Gessner, K., Markwitz, V., & Güngör, T. (2017). Crustal fluid flow in hot continental extension: tectonic framework of geothermal areas and mineral deposits in western Anatolia. Geological Society, London, Special Publications, 453(1), 289–311. doi:10.1144/sp453.7
- Govers, R., & Fichtner, A. (2016). Signature of slab fragmentation beneath Anatolia from full-waveform tomography. Earth and Planetary Science Letters, 450, 10–19. doi:10.1016/j.epsl.2016.06.014
- Gürer, Ö. F., Sarıca-Filoreau, N., Özbüran, M., Sangu, E., & Doğan, B. (2009). Progressive development of the Büyük Menderes Graben based on new data, western Turkey. Geological Magazine, 146(5), 652–673. doi:10.1017/s0016756809006359
- Hempton, M. R. (1987). Constraints on Arabian Plate motion and extensional history of the Red Sea. Tectonics, 6(6), 687–705. doi:10.1029/tc006i006p00687
- Jackson, J., & McKenzie, D. (1988). The relationship between plate motions and seismic moment tensors, and the rates of active deformation in the Mediterranean and Middle East. Geophysical Journal International, 93(1), 45–73. doi:10.1111/j.1365-246x.1988.tb01387.x
- Jolivet, L., C. Faccenna, B. Goffe, E. Burov, and P. Agard (2003). Subduction tectonics and exhumation of high-pressure metamorphic rocks in the Mediterranean orogens, American Journal of Science, 303(5), 353–409. doi:10.2475/ajs.303.5.353
- Jolivet, L., Faccenna, C., Huet, B., Labrousse, L., Le Pourhiet, L., Lacombe, O., ... Driussi, O. (2013). Aegean tectonics: Strain localisation, slab tearing and

trench retreat. *Tectonophysics*, 597-598, 1–33.  
doi:10.1016/j.tecto.2012.06.011

Kahle, H.-G., Straub, C., Reilinger, R., McClusky, S., King, R., Hurst, K., ... Cross, P. (1998). The strain rate field in the eastern Mediterranean region, estimated by repeated GPS measurements. *Tectonophysics*, 294(3-4), 237–252. doi:10.1016/s0040-1951(98)00102-4

Karamanderesi, İ. H., Helvacı C. (2003). Geology and hydrothermal alteration of the Aydın–Salavatlı geothermal field, western Anatolia, Turkey. *Turk J Earth Sci* 12:175–198.

Kaya, A. (2015). The effects of extensional structures on the heat transport mechanism: An example from the Ortakçı geothermal field (Büyük Menderes Graben, SW Turkey). *Journal of African Earth Sciences*, 108, 74–88. doi:10.1016/j.jafrearsci.2015.05.002

Kaymakci, N. (2006). Kinematic development and paleostress analysis of the Denizli Basin (Western Turkey): implications of spatial variation of relative paleostress magnitudes and orientations. *Journal of Asian Earth Sciences*, 27(2), 207–222. doi:10.1016/j.jseaes.2005.03.003

Koçyiğit, A., Yusufoglu, H., & Bozkurt, E. (1999). Evidence from the Gediz graben for episodic two-stage extension in western Turkey. *Journal of the Geological Society*, 156(3), 605–616. doi:10.1144/gsjgs.156.3.0605

Koçyiğit, A., Özacar, A., (2003). Extensional Neotectonic Regime through the NE Edge of the Outer Isparta Angle, Sw Turkey: New Field and Seismic Data. *Turkish Journal of Earth Sciences* 2, 67-90.

Koçyiğit, A. (2005). The Denizli graben-horst system and the eastern limit of western Anatolian continental extension: basin fill, structure, deformational mode, throw amount and episodic evolutionary history, SW Turkey. *Geodinamica Acta*, 18(3-4), 167–208. doi:10.3166/ga.18.167-208

- Koçyiğit, A. (2015). An overview on the main stratigraphic and structural features of a geothermal area: the case of Nazilli-Buharkent section of the Büyük Menderes Graben, SW Turkey. *Geodinamica Acta*, 27(2-3), 85–109. doi:10.1080/09853111.2014.957501
- Konak, N. (2002). Geological Map of Turkey in 1/500,000 Scale: Izmir Sheet. Publication of Mineral Research and Exploration Directorate of Turkey, Ankara.
- Konak, N., M. Şenel (2002). Geological Map of Turkey in 1/500,000 scale: Denizli Sheet, Publication of Mineral Research and Exploration Directorate of Turkey, Ankara.
- Lacassin, R., Arnaud, N., Leloup, P. H., Armijo, R., & Meyer, B. (2007). Exhumation of metamorphic rocks in N Aegean: the path from shortening to extension and extrusion. *eEarth Discussions*, 2(1), 1–35. doi:10.5194/eed-2-1-2007
- Pichon, X. L., & Angelier, J. (1979). The hellenic arc and trench system: A key to the neotectonic evolution of the eastern mediterranean area. *Tectonophysics*, 60(1-2), 1–42. doi:10.1016/0040-1951(79)90131-8
- Pichon, X. L., Angelier, J., Osmaston, M. F., & Stegena, L. (1981). The Aegean Sea. *Philosophical Transactions of the Royal Society A: Mathematical, Physical and Engineering Sciences*, 300(1454), 357–372. doi:10.1098/rsta.1981.0069
- McClusky, S., Balassanian, S., Barka, A., Demir, C., Ergintav, S., Georgiev, I., ... Veis, G. (2000). Global Positioning System constraints on plate kinematics and dynamics in the eastern Mediterranean and Caucasus. *Journal of Geophysical Research*, 105(B3), 5695–5719. doi:10.1029/1996jb900351
- Mckenzie, D. P. (1970). Plate Tectonics of the Mediterranean Region. *Nature*, 226(5242), 239–243. doi:10.1038/226239a0

- McKenzie, D. (1972). Active Tectonics of the Mediterranean Region. *Geophysical Journal International*, 30(2), 109–185. doi:10.1111/j.1365-246x.1972.tb02351.x
- Mckenzie, D. (1978). Some remarks on the development of sedimentary basins. *Earth and Planetary Science Letters*, 40(1), 25–32. doi:10.1016/0012-821x(78)90071-7
- Meijer, P. T., & Wortel, M. J. R. (1997). Present-day dynamics of the Aegean region: A model analysis of the horizontal pattern of stress and deformation. *Tectonics*, 16(6), 879–895. doi:10.1029/97tc02004
- Moeck, I. S. (2014). Catalog of geothermal play types based on geologic controls. *Renewable and Sustainable Energy Reviews*, 37, 867–882. doi:10.1016/j.rser.2014.05.032
- Moores, E. M., Robinson, P. T., Malpas, J., Xenophonotos, C. (1984). Model for the origin of the Troodos massif, Cyprus, and other mideast ophiolites. *Geology*, 12(8), 500-503. doi:10.1130/0091-7613(1985)13<668b:caromf>2.0.co;2
- Oberhänsli, R., O. Candan, and F. D. H. Wilke (2010). Geochronological evidence of Pan-African eclogites from the Central Menderes Massif, *Turkish Journal. Earth Sciences*, 19, 431–447.
- Oral, M.B., Reilinger, R., Toksoz, R. (1992). Deformation of the Anatolian block as deduced from GPS measurements. *Transactions, American Geophysical Union, EOS* 73, 120.
- Ozdemir, A., Yasar, E., & Cevik, G. (2016). An importance of the geological investigations in Kavaklıdere geothermal field (Turkey). *Geomechanics and Geophysics for Geo-Energy and Geo-Resources*, 3(1), 29–49. doi:10.1007/s40948-016-0044-0

- Özen, T., Bülbül, A., & Tarcan, G. (2012). Reservoir and hydrogeochemical characterizations of geothermal fields in Salihli, Turkey. *Journal of Asian Earth Sciences*, 60, 1–17. doi:10.1016/j.jseaes.2012.07.016
- Özgür N., Karamenderesi I.H. (2015). An update of the geothermal potential in the continental rift zone of the Büyük Menderes, Western Anatolia, Turkey. In: *Proceedings, fortieth workshop on geothermal reservoir engineering Stanford University*, pp 26–28.
- Philippon, M., Brun, J.-P., Gueydan, F., & Sokoutis, D. (2014). The interaction between Aegean back-arc extension and Anatolia escape since Middle Miocene. *Tectonophysics*, 631, 176–188. doi:10.1016/j.tecto.2014.04.039
- Phillipson, A. (1918). *Kleinasien, Handbuch der Regionalen Geologie*, edited by G. Steinmann and O. Wilckens, 5, Heidelberg.
- Purvis, M., & Robertson, A. (2004). A pulsed extension model for the Neogene–Recent E–W-trending Alaşehir Graben and the NE–SW-trending Selendi and Gördes Basins, western Turkey. *Tectonophysics*, 391(1-4), 171–201. doi:10.1016/j.tecto.2004.07.011
- Purvis, M., & Robertson, A. (2005). Miocene sedimentary evolution of the NE–SW-trending Selendi and Gördes Basins, W Turkey: implications for extensional processes. *Sedimentary Geology*, 174(1-2), 31–62. doi:10.1016/j.sedgeo.2004.11.002
- Republic of Turkey Ministry of Energy and Natural Resources (2018). 2018 Faaliyet Raporu.
- Reilinger, R. E., McClusky, S. C., Oral, M. B., King, R. W., Toksoz, M. N., Barka, A. A., ... Sanli, I. (1997). Global Positioning System measurements of present-day crustal movements in the Arabia-Africa-Eurasia plate collision zone. *Journal of Geophysical Research: Solid Earth*, 102(B5), 9983–9999. doi:10.1029/96jb03736

- Rimmelé, G., Oberhänsli, R., Goffé, B., Jolivet, L., Candan, O., & Çetinkaplan, M. (2003). First evidence of high-pressure metamorphism in the “Cover Series” evolution of SW Turkey. *Lithos*, 71(1), 19–46. doi:10.1016/s0024-4937(03)00089-6
- Roche V., Guillou-Frottier L., Jolivet L., Loiselet C., Bouchot V. (2015). Subduction and slab tearing dynamics constrained by thermal anomalies in the Anatolia-Aegean region. *Geophysical research abstracts*, vol 17.
- Roche V., Sternai P., Guillou-Frottier L., Jolivet L., Gerya T. (2016). Location of eastern Mediterranean hot springs induced by mantle heat flow due to slab roll-back and tearing. *American Geophysical Union*
- Roche, V., Sternai, P., Guillou-Frottier, L., Menant, A., Jolivet, L., Bouchot, V., & Gerya, T. (2018). Emplacement of metamorphic core complexes and associated geothermal systems controlled by slab dynamics. *Earth and Planetary Science Letters*, 498, 322–333. doi:10.1016/j.epsl.2018.06.043
- Royden, L. H. (1993). The tectonic expression slab pull at continental convergent boundaries. *Tectonics*, 12(2), 303–325. doi:10.1029/92tc02248
- Sarıca, N. (2000). The Plio-Pleistocene age of Büyük Menderes and Gediz grabens and their tectonic significance on N–S extensional tectonics in West Anatolia: Mammalian evidence from the continental deposits. *Geological Journal*, 35, 1–24. doi: 10.1002/(SICI)1099-1034(200001/03)35:13.3.CO;2-1
- Sözbilir, H. and Emre, T. (1990). Neogene stratigraphy and structure of the northern rim of the Büyük Menderes graben: International Earth Sciences Congress on Aegean Regions (IESCA-1990), Proceedings, pp. 314–322, İzmir, Turkey.
- Sun, S. (1990). Denizli-Uşak Arasının Jeolojisi ve Linyit Olanakları [Geology of the area between Denizli and Uşak and lignite occurrences] (Report No. 9985) General Directorate of Mineral Research and Exploration (MTA) [in Turkish, unpublished].

- Şarođlu, F., Y. Yılmaz (1991). Geology of the Karlıova region: Intersection of the North Anatolian and the East Anatolian transform faults, *Bull. Tech. Univ. Istanbul, Spec. Issue on Tectonics*, 44(1), 475–493.
- Şengör, A. M. C. (1979). *Turkiyenin neotektonik esasları (Neotectonics of Turkey, 2)*, Ankara: Türkiye Jeoloji Kurumu Yayınları Serisi.
- Şengör, A. M. C., & Kidd, W. S. (1979). Post-collisional tectonics of the Turkish-Iranian plateau and a comparison with Tibet. *Tectonophysics*, 55(3-4), 361–376. doi:10.1016/0040-1951(79)90184-7
- Şengör, A. M. C. (1987). Cross-faults and differential stretching of hanging walls in regions of low-angle normal faulting: examples from western Turkey. *Geological Society, London, Special Publications*, 28(1), 575–589. doi:10.1144/gsl.sp.1987.028.01.38
- Şengör, A. M. C., & Yılmaz, Y. (1981). Tethyan evolution of Turkey: A plate tectonic approach. *Tectonophysics*, 75(3-4), 181–241. doi:10.1016/0040-1951(81)90275-4
- Sengör, A. M. C., Satir, M., & Akkök, R. (1984). Timing of tectonic events in the Menderes Massif, western Turkey: Implications for tectonic evolution and evidence for pan-African basement in Turkey. *Tectonics*, 3(7), 693–707. doi:10.1029/tc003i007p00693
- Şengör, A. M. C., Görür, N., & Şarođlu, F. (1985). Strike-slip faulting and related basin formation in zones of tectonic escape: turkey as a case study. *Strike-Slip Deformation, Basin Formation, and Sedimentation*, 227–264. doi:10.2110/pec.85.37.0227
- Şimşek, Ş., (1984). Denizli-Kızıldere-Tekkehamam-Tosunlar-Buldan-Yenice alanının jeolojisi ve jeotermal enerji olanakları. *Mineral Res. Expl. Direct. Turkey (MTA), Scientific Report No: 7846*, p. 85. Ankara, Turkey (in Turkish).

- Şimşek, Ş. (1985). Geothermal model of Denizli, Sarayköy-Buldan area. *Geothermics*, 14(2-3), 393–417. doi:10.1016/0375-6505(85)90078-1
- Temel, O., B. N. Çiftci, N. Terzioğlu, and H. Sancay (2004). Edremit Körfezi dolayının jeolojisi ve Hidrokarbon olanakları (Geology of the Edremit Bay and the surroundings, and the hydrocarbon potential), TPAO Arama Dairesi Arşivi Rapor, No. 4534.
- Uzel, B., H. Sozbilir, and C. Özkaymak (2012). Neotectonic evolution of an actively growing superimposed basin in western Anatolia: The inner bay of Izmir, Turkey, *Turkish J. Earth Sci.*, 21 (4), 439–471. doi:10.3906/yer-0910-11
- Westaway, R. (1993). Neogene evolution of the Denizli region of western Turkey. *Journal of Structural Geology*, 15(1), 37–53. doi:10.1016/0191-8141(93)90077-n
- Westaway, R. (1994a). Evidence for dynamic coupling of surface processes with isostatic compensation in the lower crust during active extension of western Turkey. *Journal of Geophysical Research: Solid Earth*, 99(B10), 20203–20223. doi:10.1029/94jb01054
- Westaway, R. (1994b). Present-day kinematics of the Middle East and eastern Mediterranean. *Journal of Geophysical Research: Solid Earth*, 99(B6), 12071–12090. doi:10.1029/94jb00335
- Westaway, R. (2004). Kinematic consistency between the Dead Sea Fault Zone and the Neogene and Quaternary left-lateral faulting in SE Turkey. *Tectonophysics*, 391(1-4), 203–237. doi:10.1016/j.tecto.2004.07.014
- Yazman, M. K., A. Guven, Y. Ermis, M. Yılmaz, I. Ozdemir, Y. Akcay, U. Gonulalan, O. Tekeli, V. Aydemir, A. Sayılı, Z. Batı, H. Iztan, and O. Korucu (1998). Alaşehir Grabeni'nin ve Alaşehir-1 Prospektinin Değerlendirme Raporu, TPAO Exploration Group, unpublished technical report, Ankara.

- Yılmaz, Y. (1981). Sakarya kıtası güney kenarının tektonik evrimi (Tectonic evolution of the southern edge of the Sakarya continent), *Istanbul Yerbilimleri*, 1(1-1), 35-52 (Turkish with English abstract).
- Yılmaz, Y., Genç, Ş. C., Yiğitbaş, E., Bozcu, M., & Yılmaz, K. (1995). Geological evolution of the late Mesozoic continental margin of Northwestern Anatolia. *Tectonophysics*, 243(1-2), 155-171. doi:10.1016/0040-1951(94)00196-g
- Yılmaz, Y. (1997). *Geology of Western Anatolia, Theme 3: General geology, in Active Tectonics of Northwestern Anatolia: The Marmara Polyproject, A Multidisciplinary Approach by Space-Geodesy, Hydrology, Geothermics, and Seismology*, Vdf Hochschulverlag, Zurich.
- Yılmaz, Y., Genç, Ş. C., Gürer, F., Bozcu, M., Yılmaz, K., Karacik, Z., ... Elmas, A. (2000). When Did the Western Anatolian Grabens Begin to Develop? *Geological Society, London, Special Publications*, 173(1), 353-384. doi:10.1144/gsl.sp.2000.173.01.17
- Yılmaz, Y. (2017). Major Problems of Western Anatolian Geology. *Geophysical Monograph Series*, 141-187. doi: 10.1002/9781118944998.ch6
- Yılmaz S., Pasvanoğlu S., Vural S. (2010). The relation of geothermal resources with young tectonics in the Gediz graben (West Anatolia, Turkey) and their hydrogeochemical analyses. *Proceedings world geothermal congress*, pp 1-10.